The 436th Symposium on Sustainable Humanosphere

The 5th Asia Research Node Symposium on Humanosphere Science

Date: December 22-23, 2020
Venue: Symposium goes Online

URL: http://www.rish.kyoto-u.ac.jp/arn5/

Organized by

RISH 生存圏研究所
Research Institute for Sustainable Humanosphere, Kyoto University

Preface

The Research Institute for Sustainable Humanosphere (RISH) of Kyoto University launched a new program called the Humanosphere Asia Research Node (ARN) in 2016. This program aims to strengthen its function as a hub for international collaborative research and foster innovation in the field of humanosphere science, with the ultimate goal of delivering solutions to global-scale problems. ARN integrates various facilities and human networks in ASEAN region and Japan for consolidating the international collaborative research on “Sustainable Humanosphere”.

One of the major actions is the organization of the ARN symposium, which aims to share the concept and recent advances of Humanosphere Science, thereby fostering students and young researchers who will sustain and expand the new science. The 1st ARN Symposium on Humanosphere Science was held in Penang, Malaysia in collaboration with Universiti Sains Malaysia (USM). The 2nd symposium was held in Uji, Japan. The 3rd symposium was held in Taichung, Taiwan in collaboration with National Chung Hsing University (NCHU). The 4th symposium was held in Nanjing, China in collaboration with Nanjing Forestry University (NFU). Due to the unfolding coronavirus (COVID-19) outbreak and travel restrictions, the 5th symposium was realized as an ONLINE event without physical attendance.

The ARN Symposium covers scientific and technological advances principally in the fields of agricultural life science, wood and timber science and engineering, and radio atmospheric science and engineering together with other related sciences contributing to creating “Sustainable Humanosphere”.

We are delighted to announce that many attendees join this 5th symposium, which runs on December 22-23, 2020. In particular, many graduate students make oral and poster presentations.

Chairperson of the 5th ARN Symposium
Hiroyuki Hashiguchi
Research Institute for Sustainable Humanosphere, Kyoto University

The 5th Asia Research Node Symposium on Humanosphere Science

December 22 (Tue)

01:00UTC(10:00JST)- **Opening Ceremony**

Chair: Hiroyuki Hashiguchi

Opening address and introduction of RISH activities

Masato Shiotani

Director of Research Institute for Sustainable Humanosphere (RISH), Kyoto University

01:30UTC(10:30JST)- **Session 1**

Chair: Mamoru Yamamoto

O-01

Influence of QBO-MJO Connection on The Turbulence Variations in The TTL Observed from Equatorial Atmosphere Radar

Arlif Nabilatur Rosyidah, Nurjanna Joko Trilaksono, and Noersomadi

O-02

Observations of turbulent mixing in Tropical Tropopause Layer (TTL)

Momoko Hashino, Hiroyuki Hashiguchi, Richard Wilson, Shinya Ogino, and Junko Suzuki

O-03

Short Vertical-Wavelength Gravity Wave Activities in the Upper Troposphere Lower Stratosphere Observed with Global Navigation Satellite System Radio Occultation under Different QBO Phases

Firas Rasyad, Tri Wahyu Hadi, and Noersomadi

Coffee break (~20 min)

02:50UTC(11:50JST)- **Session 2**

Chair: Kazufumi Yazaki

O-04

The Role of Subterranean Termites on Microplastics Transport in a Terrestrial Ecosystem

Siska Anggiriani, Hiroki Yabumoto, S Khoirul Himmi, Dodi Nandika, and Tsuyoshi Yoshimura

O-05

Result Summary on the Researches of Fast Growing Platinum Teak Wood

Wahyu Dwianto, Danang S. Adi, Dwi A. Pramasari, Eka Lestari, Teguh Darmawan, Adik Bahanawan, Yusup Amin, Dimas Triwibowo, Prabu S. Sejati, Subyakto, Mohamad Gopar, Sudarmanto, Betalini S. Hapsari, Witjaksono, Ratih Damayanti, Junji Sugiyama, and Akihisa Kitamori

O-06

Development of colorless wood by two-step delignification with maintaining natural hierarchical structure

Yoshiki Horikawa, Rino Tsushima, Hirano Seiya, Kurei Tatsuki, Keiichi Noguchi, Satoshi Nakaba, and Ryo Funada

03:50UTC(12:50JST)- **Short Poster Presentation – Elevator Speech**

Chair: Suyako Tazuru

Lunch (~60 min)

05:30UTC(14:30JST)-07:00UTC(16:00JST) **Poster Session**

07:15UTC(16:15JST)- **Session 3**
Chair: Tatsuhiro Yokoyama
O-07
Upgrade of equatorial plasma bubble simulation toward coupling with GAIA model
Taichi Komoto and Tatsuhiro Yokoyama

O-08
Ground-based calibration method for pure rotational Raman lidar profiling atmospheric temperature
Yoichiro Fujita, Masanori Yabuki, Hiroyuki Hashiguchi, Toshikazu Hasegawa, and Eiji Takeuchi

O-09
The characteristics of atmospheric gravity wave at Tomohon - Indonesia
Sefria Anggarani, Tri Wahyu Hadi, and Septi Perwitasari

O-10
DDMA-MIMO observation with the MU radar
Tomoya Matsuda and Hiroyuki Hashiguchi

December 23 (Wed)

01:00UTC(10:00JST)- **Session 4**
Chair: Kenji Umemura
O-11
Evaluations of Induced Current in Human Cells for Radio Wave Safety Experiments
Mizuki Kataoka, Junji Miyakoshi, and Naoki Shinohara

O-12
Assessment of the native predator and parasitoid biological control complex on the brown marmorated stinkbug (*Halyomorpha halys*)
Matthew T. Kamiyama, Tsuyoshi Yoshimura, Kenji Matsuura, and Chin-Cheng Scotty Yang

O-13
Lignocellulose Decomposition by the Wood-boring Beetles, *Nicobium hirtum* (Coleoptera: Anobiidae)
Ni Putu Ratna Ayu Krishanti, Takuji Miyamoto, Izumi Fujimoto, Yuki Tobimatsu, Toshiaki Umezawa, and Tsuyoshi Yoshimura

O-14
Geometric Morphometric Analysis of *Coptotermes* spp. Head Capsule Shape: Demonstrating the Convolutions of Termite Pest Determination in Indonesia
Bramantyo Wikantyoso and Tsuyoshi Yoshimura

O-15
Research of finding whether buildings designed in Japan can be built in America
Zhao Jianchi and Isoda Hirosi

02:40UTC(11:40JST)- **Closing Remarks**
Presentation of Oral and Poster Awards

Closing Address
Hiroshi Isoda
Vice Director of Research Institute for Sustainable Humanosphere (RISH), Kyoto University

Poster Session (December 22 (Tue) 05:30-07:00UTC(14:30-16:00JST))

P-01
Ionospheric observations by Equatorial Atmosphere Radar during annular eclipse in December 2019
Rieko Takagi, Tatsuhiro Yokoyama, Mamoru Yamamoto, and Kornyanat Hozumi

P-02
A TEC variation parameter analyzer of MSTIDs using fully convolutional network for deep-learning instance segmentation
Peng Liu, Tatsuhiro Yokoyama, and Hiroyuki Hashiguchi

P-03
Correlation Between PM10 and Visibility During Forest Fire in Palangka Raya
Asri Indrawati, Dita Fatria Andarini, Nani Cholianawati, and Sumaryati

P-04
Smoke Propagation during Fire Season in Kalimantan and Sumatra in 2015 and 2019
Sumaryati, Dita Fatria Andarini, Nani Cholianawati, and Asri Indrawati

P-05
Analysis of low frequency disturbances in the upper troposphere and lower stratosphere observed with Equatorial Atmosphere Radar
Noersomadi

P-06
Study on adaptive clutter rejection system using external receiving antennas for the MU radar
Ryo Yabuki, Hiroyuki Hashiguchi, Issei Terada, and Mamoru Yamamoto

P-07
Development of Software-Defined Multichannel Receiver for Equatorial Atmosphere Radar (EAR)
Hiroyuki Hashiguchi, Nor Azlan Bin Mohd Aris, and Mamoru Yamamoto

P-08
Microbial decomposition ability in cool-temperate forests of contrasting soil types in Japan
Ryosuke Nakamura, Chikae Tatsumi, Hirofumi Kajino, Yutaro Fujimoto, Rei Fujii, Tomohiro Yokobe, and Naoki Okada

P-09
Wood identification of tea rooms in “Urasenke residence“ designated as an important cultural property
Suyako Tazuru and Junji Sugiyama

P-10
Feeding ecology of invasive African big-headed ant (*Pheidole megacephala*) between urban area and peri-urban forest
Ming-Hsiao Peng, Satomi Shiodera, Takashi F. Haraguchi, Masayuki Itoh, and Kok-Boon Neoh

P-11
Competitive exclusions of alien species shape the functional and species diversity in urban and rural urban interface
Yuan-Hung Chen and Kok-Boon Neoh

P-12
Development of Rectifiers for Wireless Power Transfer to Pipeline Inspection Robots

Koki Miwatashi, Naoki Shinohara, and Tomohiko Mitani

P-13
Basic Properties of Ultra-Fine-Bubble Water focusing on Electrical Charges on the Gas-liquid Interface
Yoshikatsu Ueda, Rieko Yamamoto, Tetsuji Okuda, Yomei Tokuda, Minoru Tanigaki, Naoto Nihei, and Shoichiro Hamamoto

P-14
Electric Field Sensor Impedance in Magnetized Plasma by PIC Simulation.
Ibuki Fukasawa, Hirotsugu Kojima, Yohei Miyake, Hideyuki Usui, and Satoshi Kurita

P-15
Electric field spectrum induced by plasma in the antenna
Tomoya Ito, Hirotsugu Kojima, Satoshi Kurita, and Takahiro Zushi

P-16
High-throughput evaluation of mannan content in softwood by using Fourier-transform infrared spectroscopy
Yuto Hioki, Hirano Seiya, Fuka Matsuo, Satoshi Nakaba, Ryo Funada, Yoshiki Horikawa

P-17
Hydrogen, carbon, and oxygen isotopic variations of tree-ring cellulose in Mt. Hiei, Shiga
Yoshito Katayama, Yumiko Watanabe, Zhen Li, and Takeshi Nakatsuka

Organizing Committee

RISH, Kyoto University
[General Chair] Hiroyuki Hashiguchi
Kazufumi Yazaki, Kenji Umemura, Tatsuhiro Yokoyama, Suyako Tazuru

[Administrative Staff]
Rika Kusakabe

Abstracts
Oral Session

O-01

Influence of QBO-MJO Connection on The Turbulence Variations in The TTL Observed from Equatorial Atmosphere Radar

Arlif Nabilatur Rosyidah[1], Nurjanna Joko Trilaksono[1], Noersomadi[2]

[1] Institut Teknologi Bandung, Bandung, Indonesia, [2] National Institute of Aeronautics and Space (LAPAN), Bandung, Indonesia

Abstract

Turbulence is a primary factor in the Stratosphere–Troposphere Exchange (STE) that occurred in a layer called Tropical Troposphere Layer (TTL), the transition layer between troposphere and stratosphere at 14-18.5 km above sea level. The state of TTL is one of key answer on how phenomena in troposphere and stratosphere interact. The interaction between Quasi-Biennial Oscillation (QBO) and Madden-Julian Oscillation (MJO) in previous study is closely linked in boreal winter. QBO is zonal wind oscillation in stratosphere while MJO is an eastward moving disturbance of convective system that takes part on climate variabilities in Indonesia. However, the characteristic of turbulence intensity in TTL towards interaction of QBO-MJO remain unknown because of the scarcity of observation data. This study present intensity variation of turbulence toward QBO-MJO interaction in TTL using Equatorial Atmosphere Radar (EAR) data located in Agam, West Sumatra (0.2°S, 100.32°E). The interaction is focused in extended boreal winter period (NDJFM; 5 months) and active phase MJO is defined by phase 4.Turbulent intensity (σ_{turb}) in TTL tend to have inversely proportional value toward zonal wind in 50 hPa. Generally, enhancement of σ_{turb} is observed on active phase MJO with maximum added value $0.075\ m\ s^{-1}$ in 17 km height. The value of turbulent intensity, zonal wind, and vertical wind strengthen during QBOE (QBO Easterly) rather than QBOW (QBO Westerly) and QBON (QBO Neutral) as shown in figure 1b. This enhancement associated with stronger convective and precipitation system before that caused by more unstable atmosphere in QBOE (figure 1c).

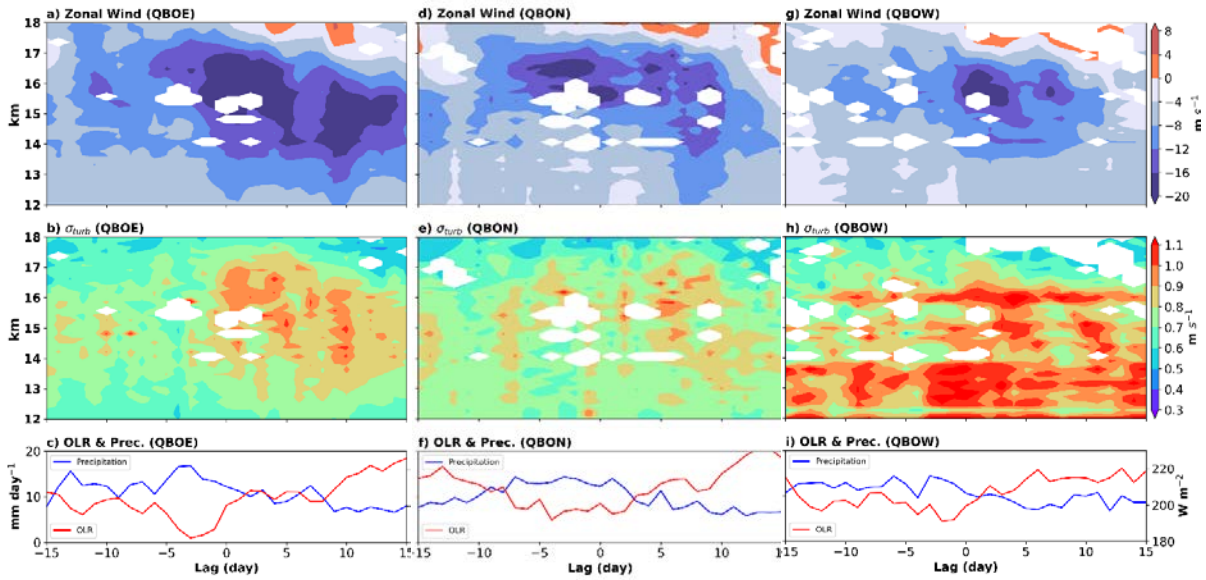

Figure 1. Zonal wind in a) QBOE, d) QBON, g) QBOW; σ_{turb} in b) QBOE, e) QBON, h) QBOW; OLR (red lines) and precipitation (blue lines) in c) QBOE, f) QBON, i) QBOW. white regions indicate sample with >90% NaN value due to low signal-to-noise ratio of the radar measurement.

O-02

Observations of turbulent mixing in Tropical Tropopause Layer (TTL)

Momoko Hashino [1], Hiroyuki Hashiguchi [1], Richard Wilson [2], Shinya Ogino [3], and Junko Suzuki [3]

[1] RISH, Kyoto University, Japan, [2] LATMOS/IPSL, France, [3] JAMSTEC, Japan

Introduction

The Tropical Tropopause Layer (TTL) is a transitional region between the troposphere and the stratosphere peculiar to the tropical zone. In recent years, the importance of elucidating the physical and chemical processes in TTL has attracted attention in terms of stratosphere-troposphere exchange (STE). Some previous studies show that there are thin (~1 km) intermittent turbulent layers in TTL, which may contribute to STE [e.g., Fujiwara et al., 2003]. However, the details of this layer have not yet been clarified because of the lack of direct observations. In this study, we (1) conducted observation campaign and analyzed turbulence and material transport as a case study and (2) investigated long-term variability of turbulent intensity using observation data from the Equatorial Atmospheric Radar (EAR).

Data

The observation campaign was conducted from November 21 to December 6, 2019, and ozone/GPS sonde observations were conducted at the Equatorial Atmosphere Observatory in West Sumatra, Indonesia. The observation data from EAR at the same station was also analyzed from 2001 to 2017. NCEP reanalysis data was used for identifying stratospheric Quasi-Biennial Oscillation (QBO) phase during the same period.

Result 1. Case study from campaign observation

During the observation campaign, turbulent layer was observed from EAR (Figure 1). From the sonde profiles (not shown), a structure thought to be equatorial Kelvin wave was found. The vertical wind shear increased as the wave amplitude increased, and the shear region also moved downward as the wave phase moved downward with time. The region of turbulent layer coincides with this shear region, and it is considered that turbulence is generated due to shear instability. At this time, the vertical distribution of ozone changed from a structure with a sharp peak to a structure that spreads vertically, so the turbulence seems to cause vertical mixing of ozone.

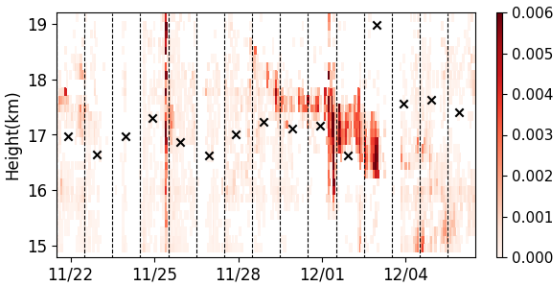

Figure 1. The eddy dissipation rate calculated from the EAR data during the observation campaign, which indicates the turbulent intensity. Cross signs indicate the tropopause height.

Result 2. Long-term analysis

Monthly average of the turbulence intensity obtained from EAR increases during winter in the northern hemisphere. On the other hand, average of the period divided according to the phase of QBO increases in the phase of westerly acceleration in upper troposphere. Both are consistent with the activity of equatorial Kelvin waves. The latter may be evidence of QBO westerly accelerating process.

References

[1] Fujiwara, M., et al., “Turbulence at the tropopause due to breaking Kelvin waves observed by the Equatorial Atmosphere Radar”, 2003, *Geophys. Res. Lett.*, 30, 1171, 2003.

O-03

Short Vertical-Wavelength Gravity Wave Activities in the Upper Troposphere Lower Stratosphere Observed with Global Navigation Satellite System Radio Occultation under Different QBO Phases

Firas Rasyad[1], Tri Wahyu Hadi[1], Noersomadi[2]

[1] Institut Teknologi Bandung, Bandung, Indonesia, [2] National Institute of Aeronautics and Space (LAPAN), Bandung, Indonesia

Gravity Waves (GWs) are believed to play important role in the generation of the driving force of the stratospheric Quasi Biennial Oscillation (QBO). Deep convections in the equatorial region can generate large amount of GWs with short vertical wavelength (λ_z <1 km) but studies of these wave activities in the upper troposphere lower stratosphere (UTLS) region are still limited due to the scarcity of high resolution atmospheric profile with global coverage. But, recent advances in Global Navigation Satellite System (GNSS) Radio Occultation (RO) retreival techniques have made it possible to derive global temperature profile with vertical resolution of less than 1 km. In this research, activities of GWs with λ_z from 0,5 to 3,5 km in the UTLS region of 20-27 km heights are identified by calculating the GW potential energy (E_p). Correlation between GW activities and QBO phases is examined using 50 hPa zonal wind as the QBO index. The results show that during both easterly and westerly QBO phases, the GW E_p value increases gradually with time and reaches its peak in the transition periods. This pattern is seen in E_p with all vertical wavelengths between 0.5-3.5 km but the percentage value of E_p for λ_z < 1 km is higher during the transition from westerly to easterly QBO. Thee GW Ep values exhibit downward propagation with the QBO phase but there are also discernible upward propagations of GW activities below 24 km height. Furthermore, large changes in QBO phase seem to occur when upward GW activities intersect the downward propagating Ep. Additionally, by comparing with El Nino Southern Oscillation (ENSO) index, even higher percentage of E_p with λ_z<1 km is also found to be associated with El Nino events.

References

Baldwin, M. P., Gray, L. J., Dunkerton, T. J., Hamilton, K., Haynes, P. H., Randel, W. J., Holton, J. R., Alexander, M. J., Hirota, I., Horinouchi, T., Jones, D. B. A., Kinnersley, J. S., Marquardt, C., Sato, K., and Takahashi, M. (2001). The quasi biennial oscillation. *Reviews of Geophysics*. doi.org/10.1029/1999RG000073.

Ern, M., Ploeger, F., Preusse, P., Gille, J. C., Gray, L. J., Kalisch, S., . . . Riese, M. (2014). Interaction of gravity waves with the QBO: A satellite perspective. Journal of Geophysical Research: Atmospheres, 119(5), 2329-2355. doi:10.1002/2013jd020731.

Geller, M. A., Tiehan Zhou, and Wei Yuan, 2016. The QBO, Gravity Waves Forced by Tropical Convection, and ENSO. Journal of Geophysical Research Atmospheres, 121, 8886-8895.

Kawatani, Y., Hamilton, K., Sato, K., Dunkerton, T. J., Watanabe, S., & Kikuchi, K. (2019). ENSO Modulation of the QBO: Results from MIROC Models with and without Nonorographic Gravity Wave Parameterization. *Journal of the Atmospheric Sciences*, *76*(12), 3893-3917. doi:10.1175/jas-d-19-0163.1.

Kursinski, E. R., G. A. Hajj, T. J. Schofield, R. P. Linfield, and K.R. Hardy, 1997. Observing Earth‘s atmosphere with radio occultation measurements using the Global Positioning System. Journal of Geophysical Research, 102, 23.429-23.465.

Lindzen, R. S., and Holton, J. R. (1968). A Theory of the Quasi-Biennial Oscillation. *Journal of the Atmospheric Sciences*. doi.org/10.1175/1520-0469(1968)025<1095:atotqb>2.0.co;2

Noersomadi, and T. Tsuda, 2016. Global Distribution of Vertical Wavenumber Spectra in the Lower Stratosphere Observed Using High-vertical-resolution Temperature Profiles from COSMIC GPS Radio Occultation. Annales Geophysicae, 34, 203-213.

Taguchi, M., 2010. Observed Connection of the Stratospheric Quasi-Biennial Oscillation with El Niño–Southern Oscillation in Radiosonde Data, J. Geophys. Res., 115, D18120, doi:10.1029/2010JD014325.

Tsuda, T., M. Nishida, C. Rocken, and R. H. Ware, 2000. A Global Morphology of Gravity Wave Activity in the Stratosphere Revealed by the GPS Occultation Data (GPS/MET). Journal of Geophysical Research, 105, 7257-7273.

Tsuda, T., X. Lin, H. Hayashi, and Noersomadi, 2011. Analysis of Vertical Wave Number Spectrum of Atmospheric Gravity Waves in the Stratosphere Using COSMIC GPS Radio Occultation Data. Atmospheric Measurement Techniques, 4, 1627-1636.

O-04

The Role of Subterranean Termites on Microplastics Transport in a Terrestrial Ecosystem

Siska Anggiriani[1], Hiroki Yabumoto[2], S Khoirul Himmi[3], Dodi Nandika[1], Tsuyoshi Yoshimura[2]

[1]IPB University, Indonesia [2]RISH–Kyoto University, Japan [3]LIPI, Indonesia

Abstract

Plastic is a widely used material for various purposes because it has many advantages such as light, cheap, strong, durable, and a good insulator for heat and electricity. On the other hand, the use of plastics has caused serious environmental pollution because of its long-time degradation characteristic of plastic. Plastic can become smaller particles due to physical, chemical, and biological factors, up to micro size. Plastics that break down into micro-sizes are called microplastics. Microplastics pollution is an important issue that has been widely researched, mainly because of its negative impact on the environment. Most of research on microplastics has focused on marine and aquatic ecosystems, while research about microplastic pollution in terrestrial ecosystem, especially its movement or transport by terrestrial organisms has not been widely conducted. Subterranean termites, soil organisms that live in terrestrial ecosystem, may contribute to the transport of microplastic particles in soil. This study aimed to explore the role of subterranean termites in transporting microplastic particles in the terrestrial ecosystem and the influence of microplastics type and size on its transport depth and transport proportion. In addition, the study also aims to assess the preference of termite species on transporting the difference type of microplastic particles.

In this study we used three types of microplastics, i.e., polyethylene (PE), polypropylene (PP), and polystyrene (PS) in three different sizes: 2–5 mm, 1–2 mm, and 0.5–1 mm, respectively. Twelve experimental stations were set up by installing PVC pipes (4 inch in diameter and 40 cm in length) vertically to the soil then filled up with sand. A bait wood made of rubber wood (5 cm x 5 cm x 2.5 cm) as well as the microplastic particles (0.2 g for each size) were put on the surface of the sand in each PVC pipe. Meanwhile, the bottom of three PVC pipes (designed as control stations) were covered by plastic net (40 mesh) as a barrier which prevents the subterranean termite from entering into the PVC pipes. The experimental stations were exposed in the field for 6 weeks since termite's attack on the wood had been observed. The distribution of microplastics in each experimental station was determined by the extraction process using aqueous flotation method. Then the depth and the percentage of microplastics transported by subterranean termites were calculated and the subterranean termites that attack wood were collected and identified.

The results showed that subterranean termites contributed to the vertical transport of microplastic particles in the terrestrial ecosystem. The transport depth of PE microplastics reached 5–10 cm depth, while the transport depth was only 0–5 cm for PP as well as PS microplastics. On the other hand, microplastic particles in control stations were not transported vertically and horizontally. The percentage of microplastic transported by subterranean termites ranged from 21.667–60%. There was significant different between type of microplastics related to termite's ability to transport it. Furthermore, microplastics transport in terrestrial ecosystem in this study was related to the foraging, tunneling, and feeding activities by subterranean termites. The subterranean termites found within the experimental stations were *Macrotermes gilvus, Odontotermes javanicus*, and *Microtermes insperatus*. However, this study also found that the most active termite species in foraging activity within the experimental stations were *M. gilvus* and *O. javanicus*.

O-05

Result Summary on the Researches of Fast Growing Platinum Teak Wood

Wahyu Dwianto [1], Danang S. Adi [1], Dwi A. Pramasari [1], Eka Lestari [1], Teguh Darmawan [1], Adik Bahanawan [1], Yusup Amin [1], Betalini S. Hapsari [2], Witjaksono[3], Ratih Damayanti[4], Junji Sugiyama[5], and Akihisa Kitamori [6]

[1] Research Center for Biomaterials,
[2] Research Center for Biotechnology,
[3] Research Center for Biology, Indonesian Institute of Sciences,
[4] Forest Products Research and Development Center, Ministry of Environment and Forestry, Indonesia
[5] Division of Forest and Biomaterials Science, Graduate School of Agriculture, Kyoto University,
[6] Faculty of Engineering, Osaka Sangyo University, Japan

Since 2006, Research Center for Biology and Biotechnology, Indonesian Institute of Sciences has developed Platinum teak, which is a superior variety of teak trees, through genetic engineering, to produce teak trees that are fast growing and are expected to have the same quality as the parent. However, information about the quality of the wood is still very limited. Therefore, it is necessary to characterize the basic properties of the wood. Wood samples were taken from three different growing sites in the Cibinong Science Center Area, Bogor. The anatomical observations, chemical component analysis, physical and mechanical property measurements of the wood have been conducted from 2015 to 2019. The results showed that anatomical observations of 5 years-old Platinum teak wood which was taken from Site 2 were not significantly different from community forests and conventional teak woods, both in their macroscopic and microscopic features. The fiber length still increased from pith to the bark, showing that the wood still consisted of juvenile wood. There were changes in the chemical components with increasing age of the wood, especially the extractive substances in alcohol-benzene and holocellulose/hemicellulose. Meanwhile, lignin and α-cellulose contents did not show a significant change with increasing wood age. This indicated that the two components were not affected by the age of the wood.

MOR and MOE of 5 years-old Platinum teak wood in Site 2 were almost the same as 20-30 years-old conventional teak wood (Table 1). Furthermore, recent researches showed that MORs of 8 to 10 years-old Platinum teak wood in Site 3 were between 75.50 - 83.11 N/mm^2 and their MOEs were between 9,221.0 - 11,565.0 N/mm^2. The value of MOR for 9 years-old Platinum teak wood which grown in Site 2 was even higher than that of 60-80 years-old conventional teak wood, i.e. 121.20 N/mm^2. From these researches it can be concluded that Platinum teak wood has very good prospects to be developed and cultivated as an alternative raw material for wood in the future and quite suitable material for timber frame structures of wooden construction with high enough strength property.

Table 1. Density, MOR and MOE values of various ages and growing sites Platinum teak wood comparing to conventional teak.

Teak Woods	MOR	MOE	Density
	N/mm^2		g/cm^3
5 years-old Platinum teak in Site 2	91.97	10,000.3	0.52
9 years-old Platinum teak in Site 2	121.20	11,898.8	0.55
8 years-old Platinum teak in Site 3	81.62	10,086.0	0.49
9 years-old Platinum teak in Site 3	83.11	11,565.0	0.50
10 years-old Platinum teak in Site 3	75.50	9,221.0	0.46
20-30 years-old conventional teak	93.43	10,338.0	0.63
60-80 years-old conventional teak	103.10	12,770.0	0.67

Acknowledgements

Author would like to thank to the Japan – ASEAN Science and Technology Innovation Platform (JASTIP) Program, which has partly funded to conduct these researches for a period of 5 years from 2015 to 2019.

O-06

Development of colorless wood by two-step delignification with maintaining natural hierarchical structure

Yoshiki Horikawa[1], Rino Tsushima[1], Hirano Seiya[1], Kurei Tatsuki[1], Keiichi Noguchi[2], Satoshi Nakaba[1], Ryo Funada[1]

[1]Institute of Agriculture, Tokyo University of Agriculture and Technology, Fuchu, Tokyo, 183-8509, Japan
[2]Institute of Technology, Tokyo University of Agriculture and Technology, Koganei, Tokyo, 184-8588, Japan

The highly controlled hierarchical structure of wood expresses the remarkable mechanical properties, which facilitate the support of the huge bodies of tress and their millenary existence. In order to create novel material that can be a filler for polymer composite, we challenged to selectively remove the lignin while maintaining its inherent structure and concluded that a two-step chemical treatment was required. The first step was alcoholysis which was conducted using ethylene glycol containing acid. The best condition was determined by using infrared spectroscopy to monitor the removal of lignin based on robust calibration model which we have reported1). The second step was bleaching wherein the delignification proceeded from the surface to the core of the wood block, and finally resulted in complete decolorization2). Although the wood block was free from lignin and hemicellulose as approximately confirmed by the chemical composition analysis, the 3-dimension colorless wood block was almost unaltered, even after freeze-drying. As a control experiment, bleaching treatment without alcoholysis was carried out. With increasing bleaching treatment, the wood was decolorized from the surface to the core. However, even after bleaching 10 times, the yellow color was still perceptible in the core, which indicates that alcoholysis was essential for obtaining the colorless block. Although the colorless wood was successfully fabricated by the two-step chemical treatment, a confirmation was required regarding its natural hierarchical structure. At first, anatomical and cell structures were observed by X-ray computed tomography (CT) which revealed that the natural cell arrangement was unaltered. Next, we recorded an X-ray diffraction diagram which indicated to maintain the microfibril orientation in the cell wall and natural crystalline structure. Finally, cellulose nanofiber was prepared using a TEMPO-mediated oxidation technique to observe the microfibril morphology. TEM image revealed that the typical shape of cellulose microfibrils without fragmentation like cellulose nanocrystal was maintained. Given the abovementioned optimal chemical treatment and structural characterization, we successfully developed a lignin-free wood block while preserving its hierarchical structure2). The lignin-free block has great potential for novel materials that are supported by a 3-dimensional wooden architecture. In addition, it will be promising specimen in that researchers can be understand the formation and functionality of the anatomical structure and lignified cell wall.

Acknowledgements
The authors sincerely appreciate Mr. Adachi of Kyoto University for providing the wood samples. The authors are also grateful to Dr. Kobayashi and Ms. Mihashi of BioJapan Industry for supporting the chemical component analysis.

References
[1] Horikawa Y, Hirano S, Mihashi A, Kobayashi Y, Zhai SC, Sugiyama J, "Prediction of lignin contents from infrared spectroscopy: chemical digestion and lignin/biomass ratios of *Cryptomeria japonica*", *Appl Biochem Biotech*, **188**, 1066-1076, 2019.
[2] Horikawa Y, Tsushima R, Noguchi K, Nakaba S, Funada R, "Development of colorless wood via two-step delignification involving alcoholysis and bleaching with maintaining natural hierarchical structure", *J Wood Sci*, **66**, 2020 on line.

O-07

Upgrade of equatorial plasma bubble simulation toward coupling with GAIA model

Taichi Komoto [1], Tatsuhiro Yokoyama[1]

[1] RISH, Kyoto, University, Japan

Research background and purpose

In recent years, as space development has advanced, high-precision, high-reliability communication, positioning, and navigation using GPS etc. are being put to practical use. The ionosphere is a transition region that connects the lower atmosphere and space, in which many artificial satellites orbit, and at the same time, that affects satellites radio waves and causes delays. The effect of radio wave delay due to the ionosphere becomes large relative to the required accuracy, and in order to correct it, there is a strong demand for understanding of the physical process of the ionosphere, the current situation, and its prediction. However, the observation means of the ionosphere are limited, and only limited temporal and spatial information can be obtained. Therefore, simulation is an effective means. Plasma bubbles are phenomena that occurs at low-latitude ionosphere. Low density region rises like bubbles due to the instability of the density stratification. Since the inside of the bubbles is very unstable and contains irregular structures, it has a great influence on the radio waves propagation. The purpose of this study is to connect the local ionospheric numerical model and the global ionospheric numerical model in a hierarchical manner, using their strength and making up for their shortcomings, and to develop a numerical model that can predict the plasma bubbles generation self-consistently. This is expected to be useful for understanding the relationship between various spatial scale phenomena and plasma bubbles generation.

Results

At this stage, we succeeded in converting the local model to whole longitude model and implementing an irregular spaces grid, and confirmed that the calculation of the potential converges at all longitudes in the high-definition model near sunset. In addition, PRE (Prereversal Enhancement) could be expressed by forcibly increasing the east-west wind that was given as a parameter. Figure 1 shows the east-west electric field calculated at an altitude of 300 km when the east-west wind is doubled from the normal case with the local time 16-20 o'clock in high definition. In the future, we aim to calculate the time evolution of plasma density and express the generation of plasma bubbles.

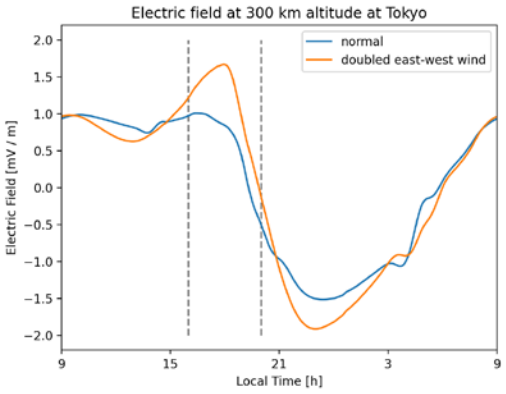

Figure 1. East-West electric field at 300km altitude.

References

[1] Yokoyama, T., Shinagawa, H., and Jin, H. (2014), Nonlinear growth, bifurcation and pinching of equatorial plasma bubble simulated by three dimensional high resolution bubble model, J. Geophys. Res. Space Physics, 119, pages 10,474 – 10,482. doi:10.1002/2014JA020708.

[2] Shinagawa, H., Jin, H., Miyoshi, Y. et al. Daily and seasonal variations in the linear growth rate of the Rayleigh-Taylor instability in the ionosphere obtained with GAIA. Prog Earth Planet Sci 5, 16 (2018). https://doi.org/10.1186/s40645-018-0175-8.

O-08

Ground-based calibration method for pure rotational Raman lidar profiling atmospheric temperature

Yoichiro Fujita [1], Masanori Yabuki[1], Hiroyuki Hashiguchi[1],
Toshikazu Hasegawa[2], and Eiji Takeuchi[2]

[1] RISH, Kyoto University, Japan, [2] EKO Instruments, Co., Ltd., Japan

Introduction

Temperature profiling in the atmospheric boundary layer is essential for understanding thermodynamic processes related to atmospheric meteorology and chemistry that induce cloud formation, heat transfer, and pollutant emission. Rotational Raman Lidar (RRL) has been developed to obtain temperature profiles with high spatiotemporal resolutions[1)]. However, it is necessary to identify its associated calibration factors to estimate the temperature during observations by comparing lidar signals with the temperature value obtained using independent measurement techniques (e.g., radiosonde). This is the main factor limiting the deployment to areas other than radiosonde observation points and long-term stable operation of RRL. In this study, we aim to establish a versatile calibration method for Raman lidar using in situ observations.

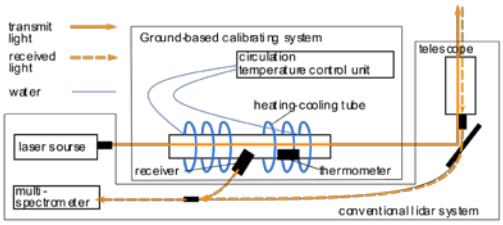

Figure 1. A ground-based calibrating system to obtain the temperature controlled rotational Raman spectrum.

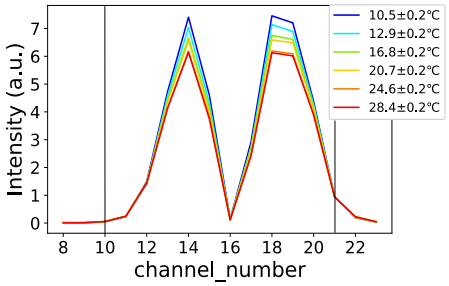

Figure 2. Rotational Raman spectrum of air in calibration system for selected temperature between 10.5 and 28.4 °C.

Ground-based calibration system

We propose a method to obtain the Rotational Raman Spectrum (RRS) on the ground in the laser irradiation area before emitting into the atmosphere, without combined measurements from other instruments. A prototype unit of the ground-based compact calibration system depicted in Figure 1 was constructed by controlling the temperature within a small detection area surrounding the laser beam path to detect the RRS at each temperature using the lidar detector. Examples of the RRS for selected air temperatures in the calibration system are shown in Figure 2. The observed RRS suggested that it is possible to distinguish the change in the spectral shape for each temperature. The calibration factors were obtained in the equivalent of radiosonde measurements under ideal conditions, regardless of weather and location. Ground-based calibration could be performed simultaneously with atmospheric measurements to observe the vertical temperature distribution. The unit will be applied for real-time continuous calibration, thereby providing a more accurate temperature estimation than conventional methods that calibrate based on comparisons with intermittent radiosonde observations. We demonstrate the preliminary results of the RRL using the proposed ground-based calibration system, including a suitable analysis method for this system associated with temperature estimation.

References

[1] Radlach, M., A. Behrendt, and V. Wulfmeyer, Scanning rotational Raman lidar at 355 nm for the measurement of tropospheric temperature fields, *Atmos. Chem. Phys.*, 8, 159–169, 2008.

O-09

The characteristics of atmospheric gravity wave at Tomohon - Indonesia

Sefria Anggarani [1,2], Tri Wahyu Hadi [2], and Septi Perwitasari [3]

[1] Earth Science Program, Institut Teknologi Bandung, Indonesia, [2]Space Science Center, LAPAN, Indoneisa, [3] NICT, Japan

Abstract

We investigate atmospheric gravity waves over Tomohon-Indonesia (1°N; 124°E) using OI 557.7 nm airglow image from 2017 to 2019. The wave parameter, horizontal wavelength, horizontal phase speed, and wave period were typically 11 – 45 km, 20 – 50 m/s, and 6 – 20 min. The seasonal variation of propagation direction is generally eastward except for the February period. The characteristic of wave propagation is mainly more influenced by the source of deep convection than background wind. From the Tropical Rainfall Measuring Mission, we derived the distribution of convective areas that occur in opposite direction with wave propagation. The background wind derived from MERRA2, approximately 20 – 30 m/s east-westward, is not strong enough to control wind filtering.

O-10

DDMA-MIMO observation with the MU radar

Tomoya Matsuda and Hiroyuki Hashiguchi

RISH, Kyoto University, Japan

1. Introduction

A phased array technique has been mainly utilized for the atmospheric radar, the wind profiling radar, and the weather radar for research objective in recent years. As an advanced usage of phased array technology, "Multiple-input multiple-output (MIMO)" technique, has been developed in the communication systems, can be applied to the radar [1]. This technique makes it possible to create the virtual antenna aperture plane beyond the actual antenna (see Figure 1), and it also possible to make the actual antenna size smaller compared to the conventional antenna with keeping the angular resolution. MIMO signal processing requires orthogonal waveforms on each transmitter to identify the transmit signals at multiple receivers, and several methods are known to realize their orthogonality [2]. To confirm the virtual antenna effect created by the MIMO technique, "Doppler Division Multiple Access (DDMA)" method is adopted to the MU radar, which can be operated as a MIMO radar with additional settings.

2. DDMA-MIMO observation with the MU radar

DDMA method is able to realize that transmit signals which have slightly different frequencies are radiated from each antenna, and they are separated at the Doppler velocity domain caused by the phase offsets at each receiver. Figure 2 shows a result of range-Doppler profiles observed by the MU radar with DDMA. This figure indicates that we can separate orthogonal transmit signals with using the MU radar, and this result leads to a virtual aperture generated by the MIMO processing will be effective.

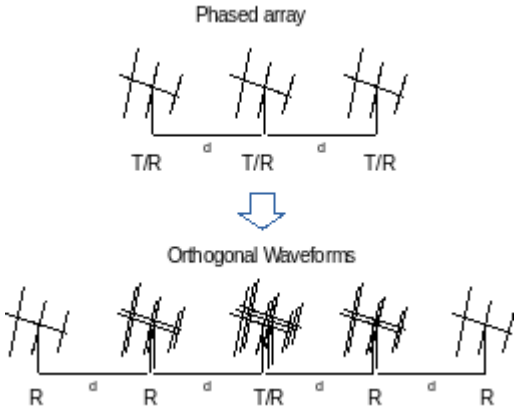

Figure 1. An image of virtual arrays corresponding to the same physical array.

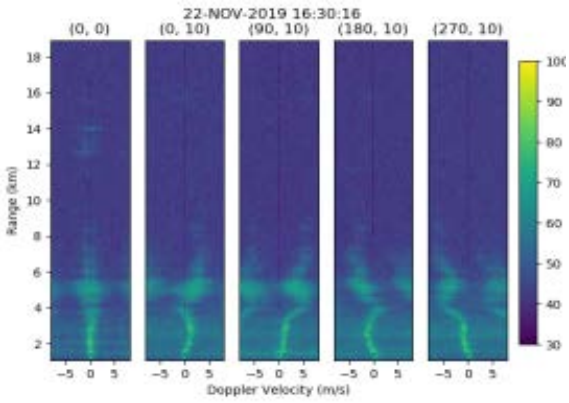

Figure 2. Range-Doppler profiles observed by the MU radar with DDMA-MIMO technique.

References

[1] M. S. Davis, G. A. Showman, and A. D. Lanterman, "Coherent MIMO radar: The phased array and orthogonal waveforms," in *IEEE Aerospace and Electronic Systems Magazine*, vol. 29, no. 8, pp. 76–91, 2014.

[2] H. Sun, F. Brigui, and M. Lesturgie, "Analysis and comparison of MIMO radar waveforms," *Int. Radar Conf. Radar 2014*, pp. 1–6, 2014.

O-11

Evaluations of Induced Current in Human Cells for Radio Wave Safety Experiments

Mizuki Kataoka [1], Junji Miyakoshi [1], and Naoki Shinohara [1]

[1] RISH, Kyoto University, Japan

Abstract

We focused on the induced current generated from electromagnetic waves that are exposed to human bodies. To demonstrate that effects, we have been developing 85 kHz and 28 GHz electromagnetic field exposing devices. The current density distributions generated by these devices are numerically obtained. The maximum value of the induced current density at 85 kHz is 9.17 A/m^2 and the current distribution is concentrated on a part of the exposed area. The maximum value at 28 GHz is 200 A/m^2 and the distribution is the concentric circle in the exposed area.

85 kHz Incubator

The 85 kHz incubator is composed of the transmitting and receiving coils which are facing the opposite side to each other. The input current is 5.8 A and the load resistance is 2 Ω. Five petri dishes are placed between the two coils. Each dish contains 10 mL of cell culture liquid (relative permittivity is 78, and conductivity is 2.08 S/m). The human cells are on the bottom of the liquid. Their size is sufficiently smaller than the wavelength that we ignore their electrical effects. We calculated the induced current in the cell culture liquid by using the simulator CST. Fig.1 shows the induced current on the bottom of the liquid. The induced current occurs strongly at the edge of the center dish and the maximum value of the current density is 9.17 A/m^2.

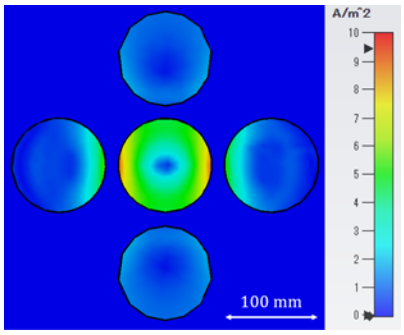

Figure 1. the induced current density distribution of 85 kHz.

28 GHz Incubator

The 28 GHz incubator has the rectangular waveguide antenna on the top center. The input power is 20 dBm. A petri dish is positioned at the lower surface. The dish includes the same cell culture liquid (the real part of complex relative permittivity is 36.6, and imaginary part of that is 31). The antenna radiates 28 GHz millimeter wave to the dish. The current density on the bottom of liquid was numerically obtained by CST. Fig. 2 illustrates the current density. The patterns of the current density make the concentric circles. Its values are from 20 A/m^2 to 30 A/m^2 and it takes larger values (up to 200 A/m^2) at the edge of the dish.

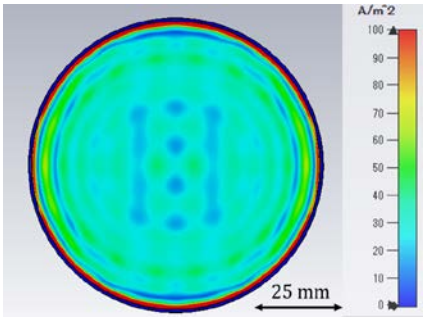

Figure 2. the current density distribution of 28 GHz.

Conclusion

We demonstrated the distribution of current densities generated by 85 kHz and 28 GHz incubators respectively. 85 kHz current distribution is concentrated on a part of the exposed area. 28 GHz current distribution is concentric circles.

O-12

Assessment of the native predator and parasitoid biological control complex on the brown marmorated stinkbug (*Halyomorpha halys*)

Matthew T. Kamiyama[1,2], Tsuyoshi Yoshimura[1], Kenji Matsuura[2], and Chin-Cheng Scotty Yang[3]

[1] RISH, Kyoto University, Japan
[2] Laboratory of Insect Ecology, Graduate School of Agriculture, Kyoto University, Japan
[3] Department of Entomology, Virginia Polytechnic Institute and State University, USA

Abstract

Brown marmorated stink bug, *Halyomorpha halys*, is a globally invasive insect pest native to East Asia (China, Japan, Korea, Taiwan) which causes major economic damage to agricultural industries in invaded regions[1]. Here, we targeted key predators and parasitoids of *H. halys* native to Japan to understand their impact on controlling the populations of the pest in its native region. Our research objectives were to determine the predatory ability of acrobat ants (*Crematogaster sp.*) on *H. halys* nymphs through lab assays, and to identify egg parasitoids of *H. halys* occurring naturally in Japan through field experiments.

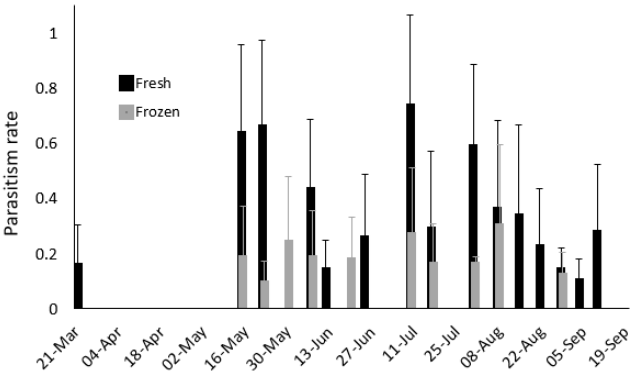

Figure 1: Parasitism rate of native parasitoids on fresh and frozen field deployed *H. halys* egg masses from March to September 2020 in Kyoto, Japan.

The two species of native *Crematogaster* ants (*C. matsumurai* and *C. osakensis*) were able to induce 100% mortality on first instar *H. halys* nymphs, and 60 – 87% on second instar nymphs. The *Crematogaster* ants, however, were unable to predate *H. halys* eggs and had only limited predatory ability on later instar (third, fourth, and fifth) nymphs. The first detection of successful *H. halys* egg parasitism was recorded in mid-March, and high parasitoid activity began in mid-May (Fig. 1). Weekly parasitism rates were highly variable ranging from 9 – 73%. The parasitoid phenology we observed in Japan of high activity beginning in the summer then lowering in the fall is similar to other *H. halys* parasitoid studies in both the native and invaded regions of *H. halys*[2,3]. Our study is the first to document field parasitism on *H. halys* as early as March for a given year.

Acknowledgements

We would like to thank the Earth Corporation, Ako Plant, for providing funding and insects for the project.

References

[1] Leskey, T. C., Hamilton, G. C., et al., "Pest status of the brown marmorated stink bug, *Halyomorpha Halys* in the USA", *Outlooks on Pest Management*, 23(5):218-226, 2012.

[2] Zhang, J., Zhang, F., et al., "Seasonal parasitism and host specificity of *Trissolcus japonicus* in northern China", *Journal of Pest Science*, 90:1127–1141, 2017.

[3] Dieckhoff, C., Tatman, K. M., and Hoelmer, K. A., "Natural biological control of *Halyomorpha halys* by native egg parasitoids: a multi-year survey in northern Delaware", *Journal of Pest Science*, 90:1143–1158, 2017.

O-13

Lignocellulose Decomposition by the Wood-boring Beetles, *Nicobium hirtum* (Coleoptera: Anobiidae)

Ni Putu Ratna Ayu Krishanti[1,2], Takuji Miyamoto[1], Izumi Fujimoto[1]
Yuki Tobimatsu[1], Toshiaki Umezawa[1], Tsuyoshi Yoshimura[1]

[1] Research Institute for Sustainable Humanosphere, Kyoto University, Japan,
[2] Research Center for Biomaterials, Indonesian Institute of Sciences, Indonesia

The digestive system of insects living in wood has long been a subject of interest. Polysacccharides degradation and also lignin modification by termites have been recently revisited by in-depth lignocellulose structure analyses using 2D NMR[1-2], however lignocellulose deconstruction in other wood-boring insects yet remain largely elusive. Therefore, this study aims to elucidate the cell wall degradation in the digestive system of the wood-boring beetle, *Nicobium hirtum*, one of the most important pests for a variety of wood products in Japan. Most of wood-boring beetles have been described to utilize only starch as a carbon source. Nevertheless, *N. hirtum* is known to nest in a wide range of hardwoods and softwoods species as its hosts. Therefore, the beetle may have an ability to digest lignocellulose components in their gut. In the present study, an integrated analyses of lignocellulose based on chemichal and 2D NMR analyses was conducted on wood (*Shorea* sp.)-contained feeds (artificial diet) and feces of *N. hirtum* larvae to reveal impacts of its digestion on hardwood lignocellulose.

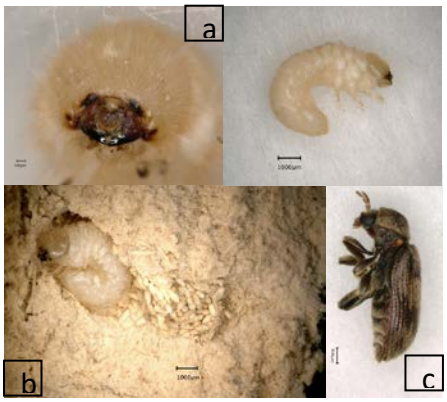

Figure 1. *Nicobium hirtum*, Anobiidae family. (a) Larva of *N. hirtum*, (b) Tunnel made inside the artificial diet by the larva, (c) *N. hirtum* adult

Twenty middle stage instar of *N. hirtum* larvae were fed with artificial diet (50% starch, 26% *Shorea* wood sawdust, and 24% yeast extract)[3]. Each larvae was placed in a hole digged in the center of a 2 x 2 x 1 cm artificial diet block and incubated in 25°C at 65% relative humidity. The feces were collected every week over 5 months to provide enough materials. The cell wall residues (CWRs)[4] for NMR and chemichal analyses were prepared from larvae feces, original artificial diet samples, and *Shorea* wood sawdust as a control. Lignocelluose composition was determined by neutral sugar analysis[5], thioglycolic acid lignin analysis[6] and analytical thioacidolysis[7,8], and solution-state 2D HSQC NMR analysis[9].

Overall, the results of both chemichal and NMR analyses showed that starch and hemicellulosic polysaccharides were preferentially decomposed over cellulose and lignin during the digestion by *N. hirtum* larvae. In addition, our data suggested that, although starch and hemicelluloses were primarily degraded, lignin also could be affected in the digestive system of *N. hirtum* larvae.

References

[1] Tarmadi et al., 2017, J Wood Sci., 63, 464; [2] Tarmadi et al., 2018, Sci. Rep., 8, 1290; [3] Kartika & Yoshimura, 2015, Insects, 6, 696; [4] Yamamura et al., 2013, Plant Biotechnol., 30, 25; [5] Miyamoto et al., 2018, Ind. Crop. Prod., 121, 124; [6] Suzuki et al., 2009, Plant Biotechnol., 26, 337; [7] Lapierre et al., 1986, Holzforschung, 40, 47; [8] Yamamura et al., 2012, Plant Biotechnol., 29, 419; [9] Mansfield et al., 2012, Nat. Protoc., 7, 1579.

O-14

Geometric Morphometric Analysis of *Coptotermes* spp. Head Capsule Shape: Demonstrating the Convolutions of Termite Pest Determination in Indonesia

Bramantyo Wikantyoso[1,2] and Tsuyoshi Yoshimura[1]

1 Research Institute for Sustainable Humanosphere (RISH), Kyoto University
2 Indonesian Institute of Sciences (LIPI)

Shape Variation Explained by Landmark-based Geometric Morphometric Analysis

The genera *Coptotermes* was composed of termites with an obvious frontal hole on their soldier caste called Fontanelle. Further differentiation of species complex relies on alates and soldier caste characters such as alates forewings, Fontanelle Seta numbers, and Head Capsule shape (HCs) [1]. Teardrop and egg-like HCs are still popularly utilized to discriminate *C. curvignathus* and *C. gestroi* in Indonesia. However, there has been no critical study to demonstrate the respective character. In this study, we conducted a geometric morphometric analysis of four described species known as pest termites existed in Indonesia namely, *C. curvignathus* (n=67), *C. gestroi* (n=82), *C. sepangensis* (n=56), and *C. kalshoveni* (n=5).

In the analysis, geometric locations of landmark were used to represent biological form. As many as 54 landmarks were collected by observing the head capsule morphology of each species under the microscope. All the landmarks were appended and subjected to the Procrustes fit and multivariate analysis (PCA, CVA, and DFA). *Coptotermes curvignathus* HCs showed lateral widening started from landmarks 11 – 50 and shrinkage started from landmarks 1 – 9 and 52 – 54 to the center. While the *C. gestroi* HCs were just the opposite shape of *C. curvignathus* and demonstrated narrowing and extension on the landmarks 11 – 50 and 1 – 9 with 52 – 54, respectively. However, in a small percentage of variance, HCSs within *C. gestroi* group also illustrated lateral widening on the landmarks 16 – 45 and narrowing on the landmarks 3 – 13 and 48 – 54. *Coptotermes sepangensis* and *C. kalshoveni* had intermediary HCs between the two formers. It seemed difficult to rely on the teardrop shape as *C. curvignathus* characteristic on the field since practitioners may encounter a similar posterior margin head capsule widening in *C. gestroi* population. It was also confirmed the perplexity *C. gestroi* determination by using HCs as the only rapid diagnostic character on the field.

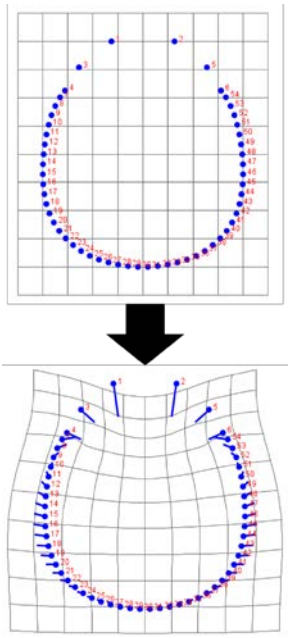

Figure 1. The transformation grid of HCs of four *Coptotermes* spp. explained by PC1 (57.24%) in multivariate analysis.

Acknowledgements

The authors would like to thank RISH, Kyoto University and the Museum Zoologicum Bogoriense, Indonesian Institute of Sciences (LIPI) for providing research facilities, equipment, and samples from Indonesia, and would like to offer heartfelt thanks also to the Japanese Ministry of Education, Culture, Sports, Science, and Technology (Monbukagakusho) for providing full funding to support the first author's master's studies at Kyoto University.

References

[1] Scheffrahn, R., T. Carrijo, J. Krecek, N.-Y. Su, A. Szalanski, J. Austin, J. Chase, and J. Mangold. 2015. A single endemic and three exotic species of the termite genus Coptotermes (Isoptera, Rhinotermitidae) in the New World. Arthropod Systematics and Phylogeny **73**:333-348.

O-15

Research of finding whether buildings designed in Japan can be built in America

ZHAO JIANCHI[1], ISODA HIROSI[2]

[1,2]RISH, Kyoto, University, Japan

Purpose and method

In this research I made some simulations of structure members in different loading conditions, to discuss whether structures which can pass the check of Japanese Standard can pass the check of American Standard or not.

Members are made of same species of wood. Members are all in same section area, load condition and load duration. The reference strength values, adjusting factors, and calculation methods are all based on each standard. First, check the capacity of each member by Japanese standard. then (1) find a smaller section to make the safety rate approach to 1, then check the capacity of this section by NDS or (2) compare the maximum load capacities calculated by different standards, to find out that the Japanese structures can be built in America or not. A part of result is in the table below, and others will be presented at the meeting.

Table 1, check the bending capacity of floor diaphragm (N/mm^2)

	reference strength	span=L=2.73m, section area: 38mm*235mm			
		live load (N/m^2)	stress	reference design value	result
JP	12	1300	2.12	10.32	pass
U.S.	9.31	1920	2.9	6.48	pass
	reference strength	span=2L=5.46m, section area: 38mm*235mm			
		live load (N/m^2)	stress	reference design value	result
JP	12	1300	8.48	10.32	pass
U.S.	9.31	1920	11.6	3.57	not pass
	reference strength	span=L=2.73m, section area: 38mm*110mm			
		live load (N/m^2)	stress	reference design value	result
JP	12	1800	12.44	12.75	pass
U.S.	9.31	2400	15.49	14.99	not pass

Conclusions

2*4 structures designed based on Japanese standard can only pass the check of NDS in some condition.

Bending members can only pass the check in America in a few condition. For the live load applied by NDS is much larger than that applied by Japanese standard.

The reference compression design value in NDS is much larger than that in Japanese standard. The compression member designed in Japan can pass check in America.

References

[1] AIJ, “Standard for Structural Design of Timber Structures”, 2006

[2] AWC, “National Design Specification for Wood Construction 2015 Edition”, 2015

[3] ASCE, “Minimum Design Loads for Buildings and Other Structures”, 2010

[4] Building Standard Law Enforcement Order, 2020

Abstracts
Poster Session

P-01

Ionospheric observations by Equatorial Atmosphere Radar during annular eclipse in December 2019

Rieko Takagi [1], Tatsuhiro Yokoyama [1], Mamoru Yamamoto [1], and Kornyanat Hozumi [2]

[1] RISH, Kyoto University, Japan, [2] NICT, Japan,

The area of the Earth's atmosphere above an altitude of about 80 km is called the ionosphere, where molecules and atoms are partially ionized. Since the electron density varies depending on altitude, time, and location, radio waves passing through the ionosphere are delayed or refracted, which cause satellite communication failures and degrade GPS positioning accuracy. It is required to monitor and predict ionospheric conditions accurately. A phenomenon called 150-km echoes is VHF radar backscatter echoes observed in the daytime near 150 km of the equatorial ionosphere. Although the generation mechanism of 150-km echoes is not yet clear, two types of echoes are known to exist: one from a naturally enhanced incoherent scattering (NEIS) process, which has a low SNR and SNR-dependent Doppler spectral width, and the other from the unstable growth of field-aligned irregularities (FAIs), which has a high SNR and SNR-independent Doppler spectral width [1]. 150 km echoes are more powerful and more frequent when the photoionizing flux from the Sun is smaller [2]. We study the equatorial ionospheric variations during the annular solar eclipse on December 26, 2019. It is known that a solar eclipse reduces the amount of sunlight when the moon passes in front of the sun in the daytime and affects the electron density distribution. We observed ionospheric irregularities in the E region with the Equatorial Atmosphere Radar (EAR) in West Sumatra, Indonesia, and the background ionospheric conditions with the ionosonde network in Southeast Asia. The annular solar eclipse occurred above the EAR between 10:18 and 14:08 local time, with the maximum obscuration at 12:11.

We conducted a special ionospheric observation by the EAR from December 25 to 27, 2019 with high time resolution by focusing on the ionospheric E region. 150-km echoes were observed on the 25th and 27th, but not on the 26th, the day of the eclipse. The eclipse probably prevented the occurrence of the 150 km echoes. The E-region echoes were observed on all three days at around 100 km altitude. Echoes were seen over a wide range of times around 90 km, and sometimes echoes were observed around 110 km. The Doppler velocity of the E-region echoes fluctuated about thirty minutes before the beginning of the eclipse. Doppler velocities became lower from about 9:30 to 11:30, increased from about 11:30 to 13:30, and then decreased again after about 13:30. The eastward component of the Doppler velocity varied more than the northward component. Scatterplots of SNR and spectral widths for 150-km echoes show a population with a high SNR and SNR-independent Doppler spectral width on the 25th and 27th when 150-km echoes occurred. This suggests that the 150-km echoes observed by the EAR are produced by FAIs. Echoes from the NEIS could not be detected due to the lack of sensitivity of the EAR. The results of ionosonde observations show that the critical frequency of the F layer fluctuated with about an hour delay from the variation of the obscuration at all sites. We will analyze and discuss the relationship between the density change observed by ionosonde and the Doppler velocity variation.

References

[1] Chau, J. L., and Erhan Kudeki. "Discovery of two distinct types of equatorial 150 km radar echoes." *Geophysical Research Letters* 40.17 (2013): 4509-4514.

[2] Patra, A. K., et al. "The solar flux dependence of ionospheric 150 km radar echoes and implications." *Geophysical Research Letters* 44.22 (2017): 11-257.

P-02

A TEC variation parameter analyzer of MSTIDs using fully convolutional network for deep-learning instance segmentation

Peng Liu [1], Tatsuhiro Yokoyama [1], Hiroyuki Hashiguchi [1]

[1] RISH, Kyoto, University, Japan

Abstract:

Medium-scale traveling ionospheric disturbances (MSTIDs) are the most typical irregularities of nighttime mid-latitude ionosphere, which are usually associated with the periodical variation of total electron content (TEC). By analyzing Detrended TEC map, provided by GEONET GPS of Geospatial Information Authority of Japan, MSTIDs are observed as wavy structures in the plasma density at F-region heights having horizontal wavelengths of 100-1,000 km. To detect MSTIDs and analyze the parameter of them automatically, we propose a fully convolutional network (FCN) based on instance segmentation network, trained by 1500 detrended TEC images from January to July of 2019. This network could detect the position of MSTIDs from Detrended TEC map with up to 85% precision, then derive out the parameters such as wavelength, central coordinates, period, direction and duration. Meanwhile, it has a real time response speed, up to 13 frames per second. So far, our research is the first one to apply the fully convolutional network to ionosphere irregularity automatic detection and analyzation.

Keywords:

TEC, ionosphere, MSTIDs, FCN, deep learning, instance segmentation

Acknowledgement

Here we would show our deepest gratitude to all previous research, this work is just standing on the shoulders of giants. First and foremost, this research would not have been possible without the database provided by Geospatial Information Authority of Japan. Then, we want to express our appreciation to LabelMe, an open source annotation tool published on the Github, Matterport™, a company that open their R-CNN source code, and OpenCV, the library we used to process the images. Last but not least, we'd like to thank all researches behind the software and libraries which this work has used.

References

[1] Makela, J.J., Otsuka, Y. Overview of Nighttime Ionospheric Instabilities at Low- and Mid-Latitudes: Coupling Aspects Resulting in Structuring at the Mesoscale. *Space Sci Rev* 168, 419–440, 2012. https://doi.org/10.1007/s11214-011-9816-6

[2] Kotake, N., Otsuka, Y., Tsugawa, T., Ogawa, T., and Saito, A., Climatological study of GPS total electron content variations caused by medium-scale traveling ionospheric disturbances, *J. Geophys. Res.*, 111, A04306, 2006, doi:10.1029/2005JA011418.

[3] He, Kaiming, Georgia Gkioxari, P. Dollár and Ross B. Girshick. “Mask R-CNN.” *2017 IEEE International Conference on Computer Vision (ICCV)*, 2980-2988, 2017.

[4] Shelhamer, Evan, J. Long and Trevor Darrell. “Fully Convolutional Networks for Semantic Segmentation.” *IEEE Transactions on Pattern Analysis and Machine Intelligence 39* , 640-651, 2017.

P-03

Correlation Between PM10 and Visibility During Forest Fire in Palangka Raya

Asri Indrawati, Dita Fatria Andarini, Nani Cholianawati, and Sumaryati

Center for Atmospheric Science and Technology, LAPAN Indonesia

Introduction

Based on previous research that has been done, about the impact of forest fire on air quality and visibility in Palangka Raya, Kalimantan, the result are obtained that during forest fires in Palangka Raya air quality has decreased until dangerous levels and reduces visibility to 0.1 km from the normal condition around 7.7 km – 6.4 km[1]. This condition was very dangerous to both human health and the environment, because visibility can be significantly associated with air quality[2], and can be taken as a highly relevant visual indicator of air pollution level[3]. This research was carried out as a continuation of previous research by focusing on correlation between PM10 and visibility, by analyzing seasonal and annual, correlation during forest fires in Palangka Raya from 2000 - 2014. The correlation will later be used to predict PM10 concentration in Palangka Raya.

Correlation Between PM10 and Visibility

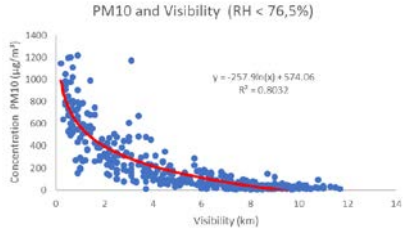

Figure 1. Correlation Between PM10 and Visibility

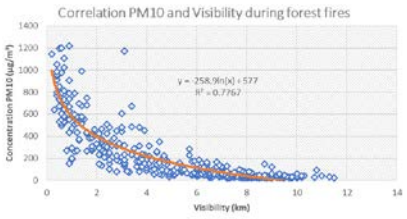

In Figure 1, the correlation between PM10 and visibility in Palangka Raya tends to form a logarithmic function. Filtering data using data limits at humidity < 76,5 %[4], with the coefficient correlation r = 0.90. The Seasonal pattern showed that the best correlation between PM10 and visibility occours in dry season (JJA and SON), with the coefficient correlation r = 0.88 (JJA) and r = 0.96 (SON). Correlation during the forest fire using concentration value above the value when there is no forest fires (normal condition), which is 23.36 µg/m³. The result showed correlation coefficient r = 0.88. The prediction of PM10 concentration using the equation from correlation PM10 and visibility during the forest fires not give a good results because the error value is still quite large, but the correlation between PM10 and PM10 prediction give a good correlation coefficient r = 0.88.

Acknowledgements

This research was funded by The Center for Atmospheric Research and Technology, Indonesian National Institute of Aeronautics and Space. We also thank to head of Palangka Raya Environmental Agency for supporting PM10 data, Ogimet for supporting visibility data.

References

[1] Sumaryati, N.Cholianawati, A. Indrawati, "The Impact of Forest Fire on Air Quality and Visibility in Palangka Raya, Kalimantan". *Journal of Physics: Theories and Applications*, Vol 3, No 1, pp:16-26, 2019.

[2] Lin, M., J. Tao, C-Y. Chen, "Regression analyses between recent air quality and visibility changes in megacities at four haze regions in China," *Aerosol and Air Quality Research*, Vol 12, No. 6, pp:1049–1061, 2012

[3] Deng, X. J., X. Tie, D. Wu et al., "Long-term trend of visibility and its characterizations in the Pearl River Delta (PRD) region, China," *Atmospheric Environment*, Vol. 42, No. 7, pp:1424–1435,2008.

[4] Apoom, N. V., C. M Shy, L. M. Neas & D. Loomis, "Estimation of particulate matter from visibility in Bangkok, Thailand", *Journal of Exposure Analysis and Environmental Epidemiology*. 11,pp: 97 – 102, 2001.

P-04

Smoke Propagation during Fire Season in Kalimantan and Sumatra in 2015 and 2019

Sumaryati, Dita Fatria Andarini, Nani Cholianawati, and Asri Indrawati

Center for Atmospheric Science and Technology, National Institute of Aeronautics and Space of Indonesia

Forest Fire in Kalimantan and Sumatera

The last of two El Nińo phenomena occurred in 2015 and 2019 have caused severe fires in Kalimantan and Sumatra during September and October. Based on hotspots observation by LAPAN, forest fires in Sumatra are found in the eastern and the southern parts of the island, and in Kalimantan fires are found all area except in the center and the eastern area. Forest fire is mostly found on peatland, that makes the burning process in a smoldering phase and produces a lot of coarse particles [1]. The aim of this paper is to study how propagate the smoke represented by its trajectory and its impact on the change of aerosol optical thickness (AOT) and visibility.

Trajectory of pollution, AOT, dan Visibility

Figure 1 is forward pollutant trajectories for two days using a matrix source of the Hysplit model. The point sources of pollutant are located in forest burned based on hotspots observation. It is seen that the wind in September is stronger than in October which formed by the smoke trajectory in September to be longer. This trajectory is formed as a result of topography of Sumatra and Kalimantan islands as well as the strong southerly wind due to high pressure in Australia in September related in winter while southerly wind is not strong in October due to spring season.

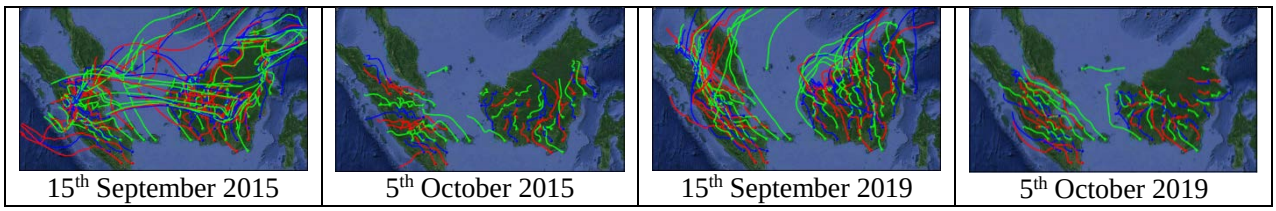

Figure 1. Smoke trajectory from Fires in Kalimantan and Sumatra starting at 11.00 UTC

Forest fires produce a lot of smoke that reduced visibility significantly [2]. The smoke-crossed area as shown in the trajectory figure increases the AOT value more than 2 and decreases in visibility more than 3 km (Fig. 2 & Fig. 3). Pollutant trajectory, AOT increasing, and visibility decreasing indicate that transboundary pollution crosses Singapore and Malaysia, especially in Peninsular Malaysia and western Serawak regions.

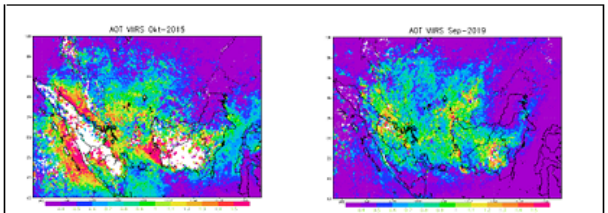

Figure 2. AOT in Oct. 2015 and Sept. 2019

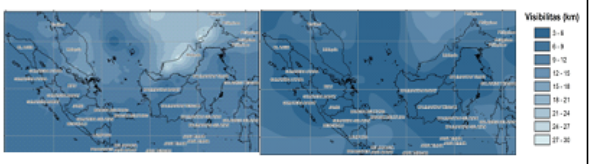

Figure 3. Visibility in Jan and Sept. 2019

Acknowledgements

This data and trajectory model used the research were supported by LAPAN, Ogimet, NASA. We thank our colleagues from LAPAN for discussing.

References

[1] Hua Y., N. Fernandez-Anez, T. E. L. Smith, and G Rein. *Int. J. of Wildland Fire*, 27, 293–312, 2018

[2] Sumaryati, N.Cholianawati, A. Indrawati, *J. Phys: Theor. Appl.*, Vol 3, No 1, pp:16-26, 2019

P-05

Analysis of low frequency disturbances in the upper troposphere and lower stratosphere observed with Equatorial Atmosphere Radar

Noersomadi

National Institute of Aeronautics and Space (LAPAN) Indonesia

Abstract

This work is the preliminary investigation of long term observation with Equatorial Atmosphere Radar (EAR) at 100.32E, 0.20S in West Sumatera, Indonesia. The analysis focuses on the variation of zonal wind (U) profile. The aim of this study is to find the index of low frequency variation of atmospheric disturbances with EAR data, particularly in the upper troposphere and lower stratosphere. The mean U at 15–17 km near tropopause showed westward wind throughout the year but it depicted semiannual oscillation. The weak westward winds were seen on April and November, while strong wind up to 13 $m.s^{-1}$ was on July. EAR observed the quasi biennial oscillation (QBO) signal around 19 km altitude. The effect of QBO to the upper troposphere is also discussed.

P-06

Study on adaptive clutter rejection system using external receiving antennas for the MU radar

Ryo Yabuki [1], Hiroyuki Hashiguchi [1], Issei Terada[1], and Mamoru Yamamoto[1]

[1] Research Institute for Sustainable Humanosphere (RISH), Kyoto University, Japan

Introduction

Strong clutter echoes from a hard target such as a mountain or building sometimes cause problems of observations with atmospheric radars. In order to reject or suppress ground clutter echoes, it is effective to use NC-DCMP (Norm Constrained-Directionally Constrained Minimum Power) method, which makes null toward the direction of the clutter, if we can receive signals independently from plural antennas [1, 2]. It has been demonstrated that the NC-DCMP method is effective to real observation data with the MU (Middle and Upper atmosphere) radar [3]. Although NC-DCMP method suppresses clutter echoes with almost maintaining the shape of main lobe to add pseudo-noise compared with the conventional DCMP method, the signal-to-noise ratio (S/N) of atmospheric echoes is somewhat degraded. We studied the clutter suppression method with little S/N degradation by using external antennas.

System and experimental result

Four turnstile antennas are installed in the MU radar site. The signal from the antenna is sent to the MU radar observation room through the coaxial cable after amplified by the low noise amplifier (LNA) with the limiter and band-pass filter (BPF). It is further amplified by the LNA in the observation room, and then down-converted to intermediate frequency (5 MHz) signal to input to the multi-channel receiving system of the MU radar. We compared the NC-DCMP method using the each received data of 25 channels, which is a conventional clutter suppression method, and the NC-DCMP method using the simple combination of 25 channels and 4 channels of external antennas. In the former case, the S/N of the atmospheric echoes is somewhat degraded, but in the latter case the main lobe shape is guaranteed by 25 channel simple synthesis, so the S/N degradation is not observed. In the latter case, the clutter suppression is sometimes insufficient. This cause is considered to be that the current positions of external antennas are biased to the north side. Antenna positions should be optimized in the future.

Figure 1. Left: MU radar antenna. Right: An example of external receiving antennas.

Future plan

We can apply the achievement of this study to the Equatorial Atmosphere Radar (EAR), which is a VHF-band active phase-array radar located at West Sumatera, Indonesia. The EAR system is the similar as the MU radar, but its receiving channel is only one. We have been developing a multichannel receiver system for the EAR using a combination of the Universal Software Radio Peripheral X300 (USRP X300) and GNU Radio software.

References

[1] Kamio, K., K. Nishimura, and T. Sato, Adaptive sidelobe control for clutter rejection of atmospheric radars, *Ann. Geophys.*, **22**, 4005-4012, 2004.

[2] Nishimura, K., T. Nakamura, T. Sato, and K. Sato, Adaptive Beamforming Technique for Accurate Vertical Wind Measurements with Multichannel MST Radar, *J. Atmos. Ocean. Tech.*, **29**, 1769-1775, 2012.

[3] Hashiguchi, H., T. Manjo, and M. Yamamoto, Development of Middle and Upper atmosphere radar real-time processing system with adaptive clutter rejection, *Radio Sci.*, **53**, doi:10.1002/2017RS006417, 2018.

P-07

Development of Software-Defined Multichannel Receiver for Equatorial Atmosphere Radar (EAR)

Hiroyuki Hashiguchi [1], Nor Azlan Bin Mohd Aris[1, 2], and Mamoru Yamamoto[1]

[1] Research Institute for Sustainable Humanosphere (RISH), Kyoto University, Japan
[2]Universiti Teknikal Malaysia Melaka (UTeM), Malaysia

Introduction

Equatorial Atmosphere Radar (EAR) is a 47-MHz Doppler radar operated with an active phased-array antenna system. It had originally been equipped with a single receiving channel system since its establishment in 2001 at the equator in Kototabang, West Sumatra, Indonesia (0.20S, 100.32E). We have developed a multichannel receiver system for the EAR using a combination of the Universal Software Radio Peripheral X300 (USRP X300) and GNU Radio software. There are a number of advantages to have multichannel receiver system such as to enable spaced-antenna method and spatial domain interferometry.

Software-defined multichannel receiver system

Two USRP X300 devices, corresponding to four receiving channels, were synchronized using 10 MHz reference clocks and a pulse per second (1 PPS) signal. The standard observation system of the EAR is retained by splitting the received echo signals through directional coupler which enabled simultaneous observation of the two different techniques, spaced-antenna and Doppler beam swinging. The signal for spaced-antenna application is fed to the USRP X300s for digital conversion, and then stored on a Hard Disk Drive (HDD). The ranging of the data is carried out by taking advantage of the leaked transmitted pulse, before demodulated and coherently integrated [1].

Experimental results

Performance analysis using multiple receiving antennas orientation for the application of spaced-antenna method on the EAR has been carried out through multiple experiments in 2019 [2]. Phase correction is applied to all channels for a single spectrum in the real time signal processing for improving the phase synchronization. The initial results show the existence of noticeable fluctuations in the estimated horizontal wind. Then, a comparison of the EAR spaced-antenna (SA) performance with five different orientations taking into consideration the size of receiving antenna and its separation distance has been presented, where the horizontal wind profiles using Full Correlation Analysis (FCA) were estimated and compared with the standard EAR data. Based on the results, the configuration with the largest aperture shows slight advantage over the other four configurations but with limited improvement.

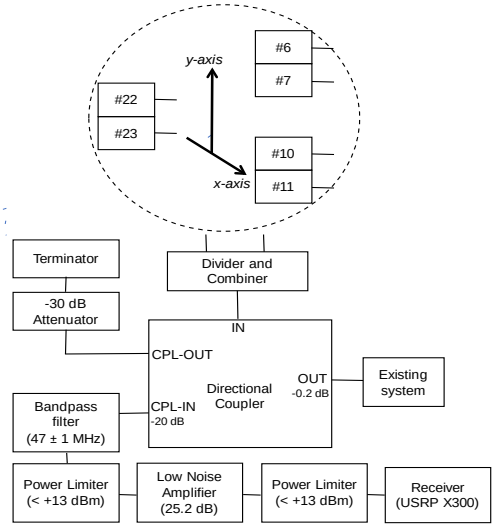

Figure 1. The configuration of the EAR multichannel receiver [2].

Future plan

If we can receive signals independently from plural antennas, ground clutter echoes can be suppressed using Norm Constrained-Directionally Constrained Minimum Power method, which makes null toward the direction of the clutter [3]. We will apply this method to the EAR multichannel receiver system.

References

[1] N. A. M. Aris, H. Hashiguchi, and M. Yamamoto, Development of software-defined multichannel receiver for EAR, *Radio Sci.*, **54**, 671-679, doi:10.1029/2019RS006817, 2019.

[2] N. A. M. Aris, H. Hashiguchi, and M. Yamamoto, Evaluation of EAR spaced-antenna performance using multiple receiving antennas orientations, *Radio Sci.*, **55**, e2019RS007049, doi:10.1029/2019RS007049, 2020.

[3] H. Hashiguchi, T. Manjo, and M. Yamamoto, Development of Middle and Upper atmosphere radar real-time processing system with adaptive clutter rejection, *Radio Sci.*, **53**, doi:10.1002/2017RS006417, 2018.

P-08

Microbial decomposition ability in cool-temperate forests of contrasting soil types in Japan

Ryosuke Nakamura[1], Chikae Tatsumi[2], Hirofumi Kajino[3], Yutaro Fujimoto[3], Rei Fujii[3], Tomohiro Yokobe[3] and Naoki Okada[3]

[1] RISH, Kyoto University, Kyoto, Japan
[2] Graduate School of Agriculture, Hokkaido University, Sapporo, Japan
[3] Graduate School of Agriculture, Kyoto University, Kyoto, Japan

Summary

There is a wide consensus that forests are key in climate change mitigation, but we still have much to learn about litter decomposition that greatly influences global carbon dynamics. This study aims to reveal how microbial decomposition ability differs among sites on contrasting rock types in Japan. The rocks greatly differ in mineral composition (e.g., karst sites on calcium rich rock, serpentine site on heavy metal rich rock).

This study was conducted in cool-temperate deciduous broadleaf forest stands of serpentine and non-serpentine sites on Mt. Oe, Kyoto and of karst and non-karst sites on Mt. Ibuki, Shiga in Japan.

We conducted a decomposition experiment by using commercially available non-woven bags (110 mm x 105 mm) that consisted of polyethylene and polypropylene (Ochappa-Pon, Cotton Labo Co., Ltd, Tokyo, Japan). To evaluate microbial decomposition ability, we used three chemically distinct substrates: nutrient-rich green tea leaves, high-quality cellulose filter paper, unbleached coffee filter paper. The bags were placed in the field in May 2020 (Fig. 1) and collected every month from June to October 2020.

Figure 1. Decomposition experiment with various substrates (green tea, cellulose filter, coffee filter) to investigate the ability of microbes to decompose organic matter.

We found that decomposition rate differed greatly among sites and substrates. In serpentine vs. non-serpentine sites, decomposition rate of green tea and cellulose filter was higher in the non-serpentine site, while decomposiiton rate of coffee filter did not differ. In karst vs. non-karst sites, decomposition rate of green tea was higher in the non-karst site, whereas decomposition rate of cellulose and coffee filters was not different. The composiiton of microbes attached to the decomposed substrates will be analyzed to explain the observed patterns of decomposiiton.

Acknowledgements

We thank landowners for allowing us to conduct our study in their land.

P-09

Wood identification of tea rooms in “Urasenke residence “ designated as an important cultural property

Suyako Tazuru [1] and Junji Sugiyama [2]

[1] RISH, Kyoto University, Japan, [2] Kyoto University, Japan

Abstract

Wood identification was performed on the 63 elements from the tea rooms such as Konnichi-an, Totsutotsusai, and so on located in the residence of the head of the Urasenke in Kyoto, Japan prior to the restoration. The aim of this study is to identify the wood species in these tea rooms designated as important cultural property for restoration and to learn wood selection of tea rooms in Urasenke which is one of the various schools of tea ceremony in Japan. This research is part of a larger project in which the wood species of tea room in Japan underwent microscopic wood identification. Aside from conventional optical microscopy, synchrotron x-ray micro-tomography for very small samples was performed for wood identification.

Our identification revealed that 16 wood species namely, *Abies* sp., *Actinidia* sp., *Betula* sp., *Carpinus* sp., *Castanea crenata, Castanopsis* sp., *Chamaecyparis obtusa*, *Chamaecyparis pisifera*, *Cryptomeria japonica*, *Magnolia* sp. (Fig. 1), *Morus bombycis*, *Pinus* subgen. Diploxylon sp., *Podocarpus macrophyllus*, *Stewartia sp., Thuja standishii* and *Thujopsis dolabrata* were used.

It was revealed that *Actinidia* sp. rare species for construction member was used on the Toko bashira and Toko gamachi in Totsutotsusai. It would be able to say that our approach could expand conventional knowledge of the Urasenke wood selection, as well as Kimura Seibei's conception of wood selection for tea ceremony room.

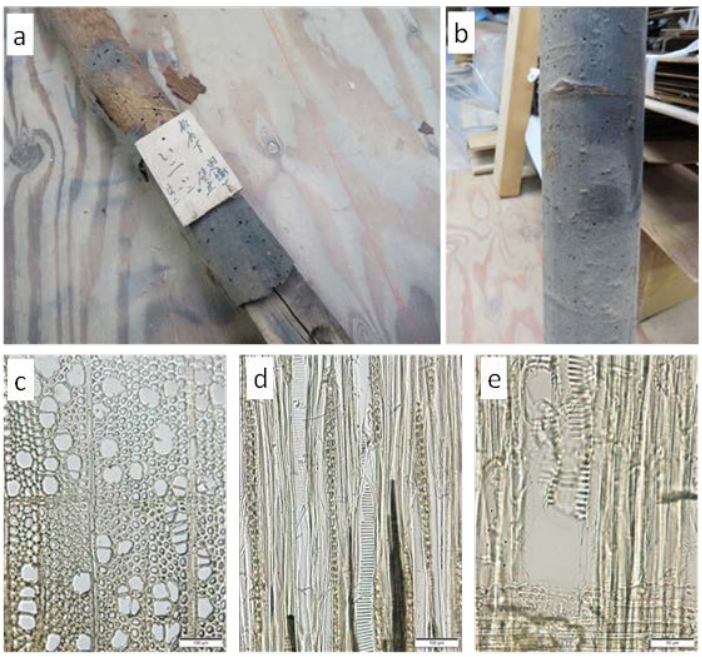

Fig. 1 Appearance of the Kabe dome in Tatami roka (No. 30) repaired in III term (a), bark of it (b) and optical micrographs of cross (c), tangential (d) and radial sections (e) of its specimen.

Acknowledgements

We are indebted to Toshiaki Hikima (Kyoto Prefecture) and Urasenke residence for providing the opportunity of investigation and for their kind cooperation and suggestions. This work was also supported by JSPS KAKENHI Grant Number 16K18730, and RISH Mission-linked Research Funding, #2017-5-4-1, #2018-5-4-1 and #2019-5-4-1.

P-10

Feeding ecology of invasive African big-headed ant (*Pheidole megacephala*) between urban area and peri-urban forest

Ming-Hsiao Peng[1], Satomi Shiodera[2,3], Takashi F. Haraguchi[4], Masayuki Itoh[5], Kok-Boon Neoh[1]

[1]Department of Entomology, National Chung Hsing University, 145, Xingda Rd. South District, Taichung 402 Taiwan
[2]Research Institute for Humanity and Nature, 457-4, Motoyama, Kamigamo, Kyoto 603-8047, Japan
[3]Center for Southeast Asian Studies, Kyoto University, 46 Shimoadachi-cho, Yoshida Sakyo-ku, Kyoto 606-8501, Japan
[4]Biodiversity Research Center, Research Institute of Environment, Agriculture and Fisheries, Osaka Prefecture, 10-4 Koyamotomachi, Neyagawa, Osaka 572-0088, Japan
[5]School of Human Science and Environment, University of Hyogo, 1-1-12 Shin-zaike, Himeji, Hyogo, 670-0092, Japan

Abstract
Pheidole megacephala is one of five ant species listed in the 100 world worst invasive species, and has caused a devastating impact on ecology and agriculture. The negative impact contributed by *P. megacephala* may be greater than any other invasive ant species given the *P. megacephala* is now widespread and omnipresent in urban and forest ecosystem. This study aims to identify factors such as feeding ecology underlying their colony expansion in urban ecosystems. We found that the isotopic values of carbon and nitrogen did not display significant difference between April and October, indicating the types of diet intake by the ant in urban and peri-urban forest were consistent across seasons. Our results indicated that the values of $\delta^{13}C$ was significant higher in urban compared with peri-urban forest. The result suggest that man-made food may be an important carbohydrate resource for ants in urban areas. In addition, *P. megacephala* population in urban areas was prone to carnivorous diet intake. The values of $\delta^{15}N$ in urban area were significantly higher compared with peri-urban forest. The artificial lights in urban area attract insect preys and thus resulting in the shift of diet of *P. megacephala* from plant-based resources to animal-based resources. A higher variation of carbon isotope signatures in urban areas relative to peri-urban forest indicated a diverse food source intake by the ants. This was further supported by the result of morphological measurement, which is more varied in urban populations. In summary, our study provides an insight into local adaption strategy of invasive ant in urban ecosystems.

References

[1] Bolton, B. (2003) *Synopsis and classification of Formicidae*. American Entomological Institute.
[2] Cogni, R. & Oliveira, P. (2004) Patterns in foraging and nesting ecology in the neotropical ant, Gnamptogenys moelleri (Formicidae, Ponerinae). *Insectes sociaux,* **51,** 123-130.
[3] Hoffmann, B.D., Andersen, A.N. & Hill, G.J. (1999) Impact of an introduced ant on native rain forest invertebrates: Pheidole megacephala in monsoonal Australia. *Oecologia,* **120,** 595-604.
[4] Hoffmann, B.D. & Parr, C.L. (2008) An invasion revisited: the African big-headed ant (Pheidole megacephala) in northern Australia. *Biological invasions,* **10,** 1171-1181.
[5] Owens, A.C., Cochard, P., Durrant, J., Farnworth, B., Perkin, E.K. & Seymoure, B. (2020) Light pollution is a driver of insect declines. *Biological Conservation,* **241,** 108259.
[6] Penick, C.A., Savage, A.M. & Dunn, R.R. (2015) Stable isotopes reveal links between human food inputs and urban ant diets. *Proceedings of the Royal Society B: Biological Sciences,* **282,** 20142608.
[7] Rico-Gray, V. & Sternberg, L.d.S.L. (1991) Carbon isotopic evidence for seasonal change in feeding habits of Camponotus planatus Roger (Formicidae) in Yucatan, Mexico. *Biotropica,* 93-95.
[8] Wetterer, J.K. (2007) Biology and impacts of Pacific Island invasive species. 3. The African big-headed ant, Pheidole megacephala (Hymenoptera: Formicidae). *Pacific science,* **61,** 437-456.
[9] Wetterer, J.K. (2012) Worldwide spread of the African big-headed ant, Pheidole megacephala (Hymenoptera: Formicidae). *Myrmecological News,* **17,** 51-62.

P-11

Competitive exclusions of alien species shape the functional and species diversity in urban and rural urban interface

Yuan-Hung Chen [1], Kok-Boon Neoh [2]

[1,2]National Chung Hsing University

Introduction of alien species had been considered major reason of extinctions. For ant, so called environmental engineer, can provide positive ecosystem function in native environment. Some of the ant species, however, were introduced to exotic environment and caused tremendous destruction on ecosystem result from their capability to strongly alter the local environment and to displace native ant assemblages. For instance, *Pheidole megacephala*, *Anoplolepis gracilipes*, *Solenopsis invicta* and *Linepithema humile*.

These high aggression and advanced competition ability of alien species, inevitably result in annihilation of local community, meanwhile drive the loss of biodiversity, which result in decline of species and functional diversity. Effect of these, may potentially undermine ecosystem functioning and ecosystem services.

To reveal the impact of alien ant species on different environment in Taipin and Tanzi, Taichung city, functional diversity and species diversity index were introduced in this study. By using pitfall trap to collect ant, 6 different locations were assessed including, urban, forest area, and invaded area, in which is dominated by invasive species. Index of functional and species diversity were produced by functional morphological trait and abundance of ant in specific area. Result shows that (1) urban and forest area share similar result, which is significantly higher than invaded area. (2) Urban and invaded area both have low functional diversity. Additionally, significant difference present between forest and urban, forest and invaded area. These results reveal that invasive ant eliminate most of native ant in dominant territory, furthermore, possibly contribute to impair of ecosystem functioning due to the low functional diversity.

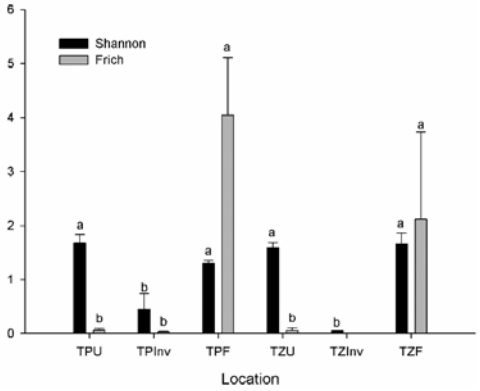

Fig. Comparison of functional richness with species diversity among Taipin and Tanzi. ShI=Shannon index. FRic=Functional richness. TPU=Urban ares of Taipin. TPF=Forest area of Taipin. TPInv=Invaded area of Taipin. TZU=Urban area of Tanzi. TZF=Forest area of Tanzi. TZInv=Invaded area of

References

[1] J. Gurevitch, D. K. Padilla, "Are invasive species a major cause of extinctions?", *Ecology and Evolution*, vol. 19, No.9, pp. 470-474, 2004.

[2] T. De Almeida, F. Mesiéard, M. Santonja, R. Gros, T. Dutoid and O. Blight, "Above- and below-gournd effects of an ecosystem engineer ant in Mediterranean dry grasslands.", *Pro. R. Soc. B*, Vol. 287, 2020.

[3] N. J. Gotelli, A. E. Arnett, "Biogeographic effects of red fire ant invasion." *Ecology Letters*, vol. 3, pp.257-261, 2000.

[4] D. P. Wojcik et al., "Red imported fire ants: impact on biodiversity." *American Entomologist*, vol. 47, pp.16-23, 2001.

[5] D. A. Holway, L. Lach, A. V. Suarez, N. D. Tsutsui, T. J. Case, "The causes and consequences of ant invasions." *Annual Review of Ecology and Systematics*, vol. 33, 181-233, 2002.

[6] R. Gaigher, M. J. Samways, S. Van Noort, "Saving a tropical ecosystem from a destructive ant-scale (Pheidole megacephala, Pulvinaria urbicola) mutualism with support from a diverse natural enemy assemblage.", *Biol invasions*, vol. 15, pp.2115-2125, 2013.

[7] M. Hill, K. Holm, T. Vel, N. J. Shah, P. Matyot, "Impact of the introduced yellow crazy ant Anoplolepis gracilipes on Bird Island, Seychelles.", *Biodiversity and Conservation*, vol. 12 pp.1969–1984, 2003.

[8] S. Carpintero, J. Reyed-López, "The role of competitive dominance in the invasive ability of the Argentine ant (Linepithema humile)", *Biol Invasions*, vol. 10, pp.25–35, 2008.

[9] R. L. Melliger, B. Braschler, H. Rusterholz, B. Baur, "Diverse effects of degree of urbanisation and forest size on species richness and functional diversity of plants, and ground surface-active ants and spiders.", *PLoS ONE*, vol. 13, 2018.

[10] M. Hejda, P. Pyšek, V. Jarošík, "Impact of invasive plants on the species richness, diversity and composition of invaded communities.", *British Ecological Society*, vol. 97, issue 3, pp.393-403, 2009.

[11] N. J. Sanders, N. J. Gotelli, N. E. Heller, D. M. Gordon, "Community disassembly by an invasive species.", *PNAS*, vol. 100, issue 5, pp.2474-2477, 2003.

P-12

Development of Rectifiers for Wireless Power Transfer to Pipeline Inspection Robots

Koki Miwatashi [1], Naoki Shinohara [1], and Tomohiko Mitani [1]

[1] RISH, Kyoto University, Japan,

Introduction

A novel method of pipeline inspection from inside by robots efficiently has been attracted attention and put to practical use. The robot is powered by a battery, and can only run a limited distance. We proposed a new system using microwave wireless power transfer for charging the batteries of inspecting robots via gas pipes. The schematics of the system is shown in Fig. 1[1]. The basic frequency of this system is 2.45 GHz. Also, the received power to the robot is assumed to be 21.4 W in this system. The proposed rectenna for this system is shown in Figure 2. The area used for a rectifier is the back side of the antenna. It is a trapezoid with an upper side of 1.9 cm, a lower side of 5.0 cm, and a height of 5.0 cm as shown in Fig. 3. In this study, a rectifier circuit is designed to fit within this size.

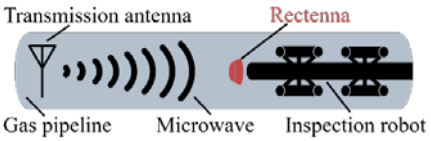

Fig. 1. Proposed MWPT system.

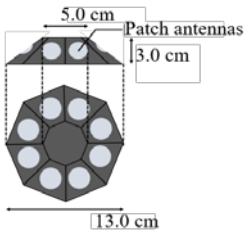

Fig. 2. Proposed rectenna

Design and Measurement of a Rectifier

The designed rectifier is shown in Fig. 4. This circuit is composed of microstrip lines with 1.1 mm width. Their characteristic impedance was 50 Ω. NPC-F260A (Nippon Pillar Packing co., ltd) is used as a substrate and its relative dielectric constant ε_r is 2.55.

We measured the characteristics of the fabricated rectifier and compared with simulation results as shown Fig. 5. RF-DC efficiency of more than 80 % was achieved at input power 3.0-5.0 W. Maximum RF-DC efficiency of 80.6 % with 3.5 W of input power and 170 Ω of load resistance. Output power of 2.82 W was obtained with input power of 3.5 W and load resistance of 170 Ω. Therefore, the total power is larger than the required power 21.4 W.

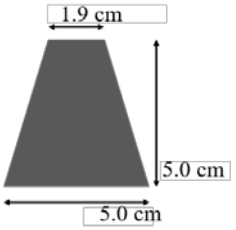

Fig. 3. Rectifier's limitation.

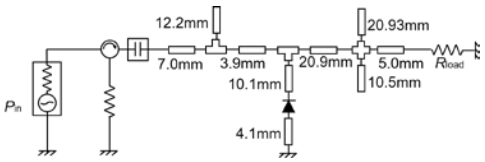

Fig. 4. Schematic of Designed Rectifier

Conclusion

We designed a 2.45GHz rectifier for WPT system for pipeline inspection robot. The designed rectifier got max RF-DC efficiency of 80.6 % with 3.5 W and 170 Ω. We showed feasibility of a rectifier for the proposed WPT system.

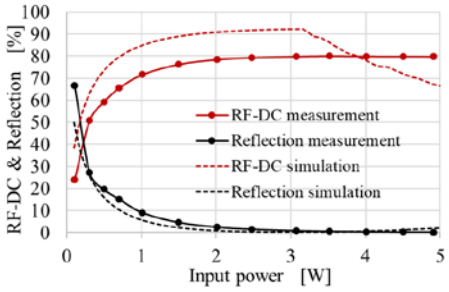

Fig. 5. RF-DC efficiency depending on P_{in} with fixed R_{load}=190 Ω.

References

[1] I. Sato and N. Shinohara, "Study on Antennas for Wireless Power Transfer to In-Line Inspection Robots," *IEEE MTT-S WPTC*, London, 2019.

P-13

Basic Properties of Ultra-Fine-Bubble Water focusing on Electrical Charges on the Gas-liquid Interface

Yoshikatsu Ueda[1], Rieko Yamamoto[1], Tetsuji Okuda[2], Yomei Tokuda[3], Minoru Tanigaki[4], Naoto Nihei[5] and Shoichiro Hamamoto[6]

[1]RISH, Kyoto University, [2]Ryukoku University, [3]Shiga University,
[4]KURNS, Kyoto University, [5]Fukushima University, [6]The University of Tokyo

Several hypotheses have been proposed to explain the stabilization mechanism of ultra fine bubbles (UFB), such as adhesion of hydrophobic substances and stabilization by dissolved ions in the vicinity. Particularly for sub-micron scale bubbles, it is difficult to see and observe them directly, and the debate about the stabilization mechanism continues. In our study, we will integrate the theory of UFB stabilization from the micro to nano scales, including scale coupling and the phenomena occurring at the liquid-gas interface, to understand the properties of UFB, especially electromagnetically and chemically. Specifically, we will first focus on sub-micron scale UFBs and investigate their charge and bubble distribution (grain shape and concentration), and accumulate data on their temporal variation including internal pressure and size, as well as their correlation with water characteristics (e.g. pH and conductivity). Changes in the internal pressure and the electromagnetic environment at the interface will be measured by using radionuclide perturbation angle correlation. The chemical properties of the bubbles will be evaluated by evaluating the reaction characteristics of radicals generated during the collapse and annihilation of bubbles and improving the chemical reactivity of the bubbles.

The stability of UFB in water is generally related to buoyancy, surface tension and solubility. In particular, the contribution of buoyancy is significant in MB scale, and other stresses may be negligible in the time scale, but in sub-micron scale UFBs, electromagnetic forces should not be neglected. As an example, the relationship between the charge (zeta potential) of the UFB and the pH of the water is shown in figure. We found that there is a some variability in oxygen UFBs related to the pH. In this study, the parameters that contribute to the stabilization of FB were widely investigated and the cross-correlated parameters were traced by simultaneous measurements of the particle size/concentration, internal pressure, chargeability and water characteristics of the UFB.

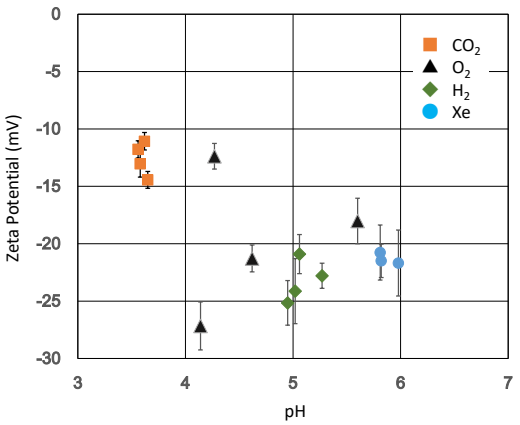

Fig. The relationship between the amount of charge in UFB and the pH of UFB water. Only oxygen has a variance.

References

[1] Y. Ueda, Y. Tokuda, H. Shida, Analysis on XAFS for Xe ulfra fine bubbles in pure water, Radiation Physics and Chemistry, Volume 176,2020,109071,ISSN0969-06X

P-14

Electric Field Sensor Impedance in Magnetized Plasma by PIC Simulation

Ibuki Fukasawa[1], Hirotsugu Kojima[1], Yohei Miyake[2], Hideyuki Usui[2] and Satoshi Kurita[1]

[1] RISH, Kyoto, University, Japan
[2] Graduate School of System Informatics, Kobe University, Japan

Antenna impedance is important because of data calibration

A dipole antenna has been commonly used as electric-field sensors to observe plasma waves in space plasma. To calibrate electric field measurements, we have been using the assumption that wavelengths are much longer than antenna lengths. However, in the next generation of satellite projects, it is possible that the wavelength is comparable to antenna length and it significantly affects the interpretation of the observation results. To understand the electric field sensor response of plasma waves with short wavelengths is significant in evaluating intensities and phases of targeted electrostatic waves. In this research, we simulated the antenna impedances of electric field sensors in magnetized plasmas over electromagnetic waves with short wavelengths. We conducted Particle-In-Cell simulations with electric field sensors as inner boundaries.[1]

The shape of the antenna impedance varies with cyclotron frequency

According to the calculation results, when the wave number of the antenna resonance is large enough, it is estimated that the resonances are seen at the frequencies of the electron cyclotron harmonics, that are frequently observed in the magnetized plasmas. The results show in some situations that at near the UHR(Upper Hybridge Resonance) frequency, one or two peaks of the antenna impedance was observed as Figure 1.

We also performed simulations to examine effects of a satellite body to characteristics of electric field sensors. When the length of the satellite parallel to the antenna was about the same as the sensor length, the resonance of the antenna impedance at the second harmonic disappeared, and the resonance at the third harmonic became prominent.

In the present paper, we discuss the characteristics of electric field sensors in plasmas over plasma waves with short wavelengths that are comparable with lengths of electric field sensors.

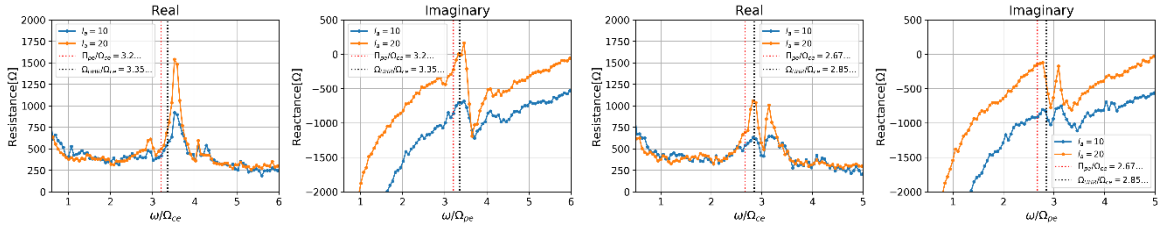

Figure 1. Antenna impedance when ωc= 0.25 and Πpe = 0.8 (left) and when ωc= 0.30 and Πpe = 0.8 (right)

References

[1] Miyake, Yohei, and Hideyuki Usui. "New electromagnetic particle simulation code for the analysis of spacecraft-plasma interactions." *Physics of Plasmas* 16.6 ,2009

P-15

Electric field spectrum induced by plasma in the antenna

Tomoya Ito [1], Hirotsugu Kojima[1], Satoshi Kurita[1] ,and Takahiro Zushi[2]

[1] RISH, Kyoto, University, Japan, [2] National Institute of Technology, Nara College, Japan

Electron temperature and density as measurement parameters in satellite observation of space plasma is important to consider physical phenomena. In Japan, particle observers are installed on artificial satellites to measure these parameters and measure them. However, it is difficult to obtain the temperature and density of cold electrons below the charged potential of the satellite from the particle observers. On the other hand, in Europe, the plasma wave observing instrument is used to obtain the electron temperature and plasma density from the spectral structure around the plasma frequency and wide-range hybrid frequency [1]. Such a plasma wave observer is called a Thermal Noise Receiver, and it is necessary to observe even a very low level spectrum, so we have to suppress the noise level generated in the observer. In order to suppress the noise level of the receiver, a low noise amplifier and a narrow band filter are indispensable, but the size of the receiver becomes large. The purpose of this research is to reduce the size of a receiver that requires such a large resource by using an analog ASIC. In this paper, we derive the signal level induced in the electric field antenna by the theoretical and numerical analysis in order to obtain the specifications required for the chip [2][3]. The assumed plasma state is a one-component Maxwell distributed electron plasma and a two-component Maxwell distributed electron plasma. For each state, we assume the magnetic field has a large influence (for example, the inner magnetosphere) [4], and the magnetic field has no influence (weak) (for example, the solar wind and the tail of the earth's magnetosphere) [5]. From the derived induced voltage level, the noise level required for the receiver is derived using the characteristics of the antenna. The electric field antenna is a dipole type antenna normally used in Japan. From this result, we will study the design policy of the analog chip that realizes the obtained noise level.

References

[1] MAKSIMOVIC, M., et al., *J. Geophys. Res.*, 100.A10: 19881-19891, 1995.
[2] SCHIFF, M. L., *Radio Science*, 5.12: 1489-1496, 1970.
[3] SENTMAN, D. D., *J. Geophys. Res.*, 87.A3: 1455-1472, 1982.
[4] MEYER-VERNET, N., *J. Geophys. Res.* 84.A9: 5373-5377, 1979.
[5] MEYER-VERNET et al., *J. Geophys. Res.*, 94.A3: 2405-2415, 1989.

P-16

High-throughput evaluation of mannan content in softwood by using Fourier-transform infrared spectroscopy

Yuto Hioki, Hirano Seiya, Fuka Matsuo,
Satoshi Nakaba, Ryo Funada, Yoshiki Horikawa

Institute of Agriculture, Tokyo University of Agriculture andTechnology,
Fuchu, Tokyo, 183-8509, Japan

The massive consumption of fossil fuels causes significant global problems such as a shortage of available energy resources and global warming derived from excessive carbon dioxide emissions, and therefore it has raised expectations for renewable energy sources. Lignocellulosic biomass from wood is a promising alternative resource for industrial chemical products and liquid fuels because it contains large amounts of sugars in the form of cellulose and hemicellulose. For converting these biomasses into cellulosic materials, a process involving efficient saccharification followed by fermentation and chemical treatments is required to separate cellulose from hemicellulose, especially in glucomannan that is major component in softwood. The glucomannan content of biomass has been measured by chemical analysis and histochemical analysis. The former is sugar analysis which can be quantitative assessment, but the geometric information is not obtained. The latter is microscopic observation with using specific antibody which enables to acquire the information on anatomical structure, but it is just qualitative analysis. In addition, both measurements are a labor- and time-intensive process. Then, alternative rapid and easy techniques for measuring glucomannan content is required.

Infrared spectroscopy is a useful technique that can detect the functional groups in organic compounds. For quantitative analysis, the sample is mixed with potassium bromide (KBr) and made to form a tablet because KBr does not absorb IR light. However, it is hygroscopic that the IR spectrum is significantly influenced by the absorption of water, thus interfering accurate measurements. An attenuated total reflectance (ATR) accessary enables for simple measurements without complex sample preparation, as the spectrum can be acquired by putting the specimen on a diamond crystal plate. When microscopic-ATR accessary is employed, it allows to survey the spectral information with the resolution of micrometer-order. ATR is a type of reflectance measurement technique, where the band intensities at lower wavenumber are increased compared to those at higher one. Therefore, multivariate analysis such as partial least square (PLS) regression after spectral pretreatment is conducted to build a better calibration model1). However, complicated mathematical algorithms using the various parameters makes it difficult for other researchers to exploit the model.

Given this background, we have challenged to develop a simple and robust calibration model for determining the relative mannose contents in softwood samples using an FTIR system equipped with ATR. Based on the assignments of the specific IR bands in the literature and measurements of standard samples2), key bands of mannan were determined. Then, a calibration curve was established using the intensity of the IR absorbance specific to mannose and assessed it by comparing the value estimated through chemical sugar analysis.

References

[1] Horikawa Y, Imai T, Takada R, Watanabe T, Takabe K, Kobayashi Y, Sugiyama J, “Chemometric analysis with near-infrared spectroscopy for chemically pretreated *Erianthus* toward efficient bioethanol production” *Appl Biochem Biotechnol*, **166**, 711-721, 2012.

[2] Horikawa Y, Hirano S, Mihashi A, Kobayashi Y, Zhai SC, Sugiyama J, “Prediction of lignin contents from infrared spectroscopy: chemical digestion and lignin/biomass ratios of *Cryptomeria japonica*” *Appl Biochem Biotech*, **188**, 1066-1076, 2019.

P-17

Hydrogen, carbon, and oxygen isotopic variations of tree-ring cellulose in Mt. Hiei, Shiga

Yoshito Katayama[1], Yumiko Watanabe[1], Zhen Li[2], Takeshi Nakatsuka[2]

[1] Graduate School of Science, Kyoto University, Kyoto, Japan
[2] Graduate School of Environmental Studies, Nagoya University, Nagoya, Japan

Isotopic fluctuations of tree-ring cellulose in Mt. Hiei

The oxygen isotopic composition of tree-ring cellulose is often used as paleoclimate proxy. We measured hydrogen, carbon, and oxygen isotope ratios of Cryptomeria japonica in Mt. Hiei, Shiga from 1663 to 2012. We observed positive anomaly of δD and negative anomaly of $\delta^{18}O$ around 1960s. They are caused by f-value fluctuation, which is defined as proportion of hydrogen/oxygen atoms in carbohydrate exchanged with xylem water during post-photosynthetic processes before cellulose synthesis (Nakatsuka et al., 2020). We therefore attempted to correct the physiological fluctuation on $\delta^{18}O$ caused by f-value fluctuation. Positive anomaly of $\delta^{13}C$ was observed around 1970s. This anomaly coincides with previous research in several regions of central Japan (Shou et al., 2009).

In this presentation, we will report the results of correlation analyses between meteorological data and $\delta^{18}O$ with/without the correction of the physiological fluctuation.

Acknowledgements

We would like to express our appreciation to Prof. Sugiyama, Prof. Tazuru and Prof. Tagami for providing us this precious study opportunity. We would like to thank Mr. Sorimachi and Mr. Adachi (RISH, Kyoto University) for cutting and polishing samples.

References

[1] Nakatsuka, T., Sano, M., Li, Z., Xu, C., Tsushima, A., Shigeoka, Y., Sho, K., Ohnishi, K., Sakamoto, M., Ozaki, H., Higami, N., Nakao, N., Yokoyama, M., Mitsutani, T., "A 2600-year summer climate reconstruction in central Japan by integrating tree-ring stable oxygen and hydrogen isotopes", *Climate of the Past*, vol. 16, no. 6, pp. 2153-2172, 2020.

[2] Sho, K., Takahashi, H.A., Miyai, H., Ikebuchi, S., Nakamura, T., "Tree-ring width and stable carbon isotope composition of Japanese cypress in the Lake Biwa area, central Japan, and their hydrologic and climatic implications", IAWA Journal, vol. 30 no. 4, pp. 395-406, 2009.


Humanosphere Asia Research Node
ARN